Atmos. Chem. Phys. Discuss., 12, 2303–2353, 2012
www.atmos-chem-phys-discuss.net/12/2303/2012/
doi:10.5194/acpd-12-2303-2012

Atmospheric Chemistry and Physics Discussions

Sulfur isotope fractionation during heterogeneous oxidation of SO_2 on mineral dust

E. Harris[1], B. Sinha[1,2], S. Foley[3], J. N. Crowley[4], S. Borrmann[1], and P. Hoppe[1]

[1]Abteilung Partikelchemie, Max-Planck-Institut für Chemie, Hahn-Meitner-Weg 1, 55128 Mainz, Germany
[2]Department of Earth Sciences, Indian Institute for Science Education and Research IISER Mohali, Sector 81, SAS Nagar, Manauli PO 140306, India
[3]Earth System Science Research Centre, Institute for Geosciences, University of Mainz, Becherweg 21, 55128 Mainz, Germany
[4]Abteilung Luftchemie, Max-Planck-Institut für Chemie, Hahn-Meitner-Weg 1, 55128 Mainz, Germany

Received: 9 January 2012 – Accepted: 11 January 2012 – Published: 25 January 2012

Correspondence to: B. Sinha (baerbel.sinha@mpic.de)

Published by Copernicus Publications on behalf of the European Geosciences Union.

Abstract

Mineral dust is a major fraction of global atmospheric aerosol, and the oxidation of SO_2 on mineral dust has implications for cloud formation, climate and the sulfur cycle. Stable sulfur isotopes can be used to understand the different oxidation processes occurring on mineral dust. This study presents measurements of the $^{34}S/^{32}S$ fractionation factor α_{34} for oxidation of SO_2 on mineral dust surfaces and in the aqueous phase in mineral dust leachate. Sahara dust, which accounts for ~60 % of global dust emissions and loading, was used for the experiments.

The fractionation factor for aqueous oxidation in dust leachate is $\alpha_{leachate} = 0.9917 \pm 0.0046$, which is in agreement with previous measurements of aqueous SO_2 oxidation by iron solutions. This fractionation factor is representative of a radical chain reaction oxidation pathway initiated by transition metal ions. Oxidation on the dust surface at subsaturated relative humidity (RH) had an overall fractionation factor of $\alpha_{het} = 1.0096 \pm 0.0036$ and was found to be almost an order of magnitude faster when the dust was simultaneously exposed to ozone, light and RH of ~40 %. However, the presence of ozone, light and humidity did not influence isotope fractionation during oxidation on dust surfaces at subsaturated relative humidity.

A positive matrix factorization model was used to investigate surface oxidation on the different components of dust. Ilmenite, rutile and iron oxide were found to be the most reactive components, accounting for 85 % of sulfate production with a fractionation factor of $\alpha_{34} = 1.012 \pm 0.010$. This overlaps within the analytical uncertainty with the fractionation of other major atmospheric oxidation pathways such as the oxidation of SO_2 by H_2O_2 and O_3 in the aqueous phase and OH in the gas phase. Clay minerals accounted for roughly 12 % of the sulfate production, and oxidation on clay minerals resulted in a very distinct fractionation factor of $\alpha_{34} = 1.085 \pm 0.013$. The fractionation factors measured in this study will be particularly useful in combination with field and modelling studies to understand the role of surface oxidation on clay minerals and aqueous oxidation by mineral dust and its leachate in global and regional sulfur cycles.

ACPD
12, 2303–2353, 2012

1 Introduction

Mineral dust represents the dominant mass fraction of atmospheric particulate matter, and it is responsible for a large amount of the uncertainty associated with aerosol climate forcing effects. Dust is important for heterogeneous chemistry, human health, visibility, ocean nutrification, and cloud formation. Mineral dust emissions are estimated to be between 1000 and 2150 Tg yr^{-1}, resulting in a global dust load of 8 to 36 Tg (Zender et al., 2004; Tanaka and Chiba, 2006). Dust emissions are expected to increase due to erosion, mining and industrial activities, overgrazing and shifting precipitation patterns (Dentener et al., 1996). Mineral dust properties are altered during transport, as finer clays are transported far from source regions relative to coarse particles, and dust particles are chemically aged by uptake of gas-phase species and heterogeneous reactions (Morales, 1986; Kim and Park, 2001; Park et al., 2004; Zhu et al., 2010).

The uptake of sulfate on to mineral dust is important both for dust properties and for the sulfur cycle. Freshly-emitted Sahara dust is very hydrophobic (Kaaden et al., 2009), whereas sulfate-coated mineral dust has increased CCN activity and may even act as "giant CCN" (Levin et al., 1996), while sulfate coatings reduce the ice nuclei activity of mineral dust (Cziczo et al., 2009; Pruppacher and Klett, 1997). Mineral dust is a particularly important source of iron in nutrient-limited open ocean waters, and chemical aging can reduce the pH of dust, increasing the solubility and bioavailability of iron (Jickells et al., 2005; Gasso et al., 2010; Rubasinghege et al., 2010; Kumar et al., 2010). Heterogeneous oxidation of SO_2 on dust can lead to reductions of $>50\,\%$ in SO_2 concentration, and may account for 50–70 % of sulfate production in dust source regions (Dentener et al., 1996; Xiao et al., 1997; Zhu et al., 2010). Coagulation on to dust can also remove sulfuric acid aerosol and gas from the atmosphere. This means that dust reduces homogeneous nucleation of H_2SO_4 and changes the size distribution of sulfur towards coarse particles, reducing its lifetime compared to sulfate in finer particulate. It is estimated that heterogeneous reactions on mineral dust reduce sulfate and nitrate aerosol cooling near dust source regions by 0.5–1 W m^{-2} (Dentener

ACPD
12, 2303–2353, 2012

et al., 1996; Liao and Seinfeld, 2005). Understanding the uptake and oxidation of SO_2 on mineral dust is a key part of investigating the interactions and feedbacks between dust, sulfur, climate and clouds.

Sulfur isotopes have been used to investigate homogeneous and aqueous oxidation of SO_2 by OH, H_2O_2 and O_3 (Harris et al., 2012). Sulfur isotope abundances are described by the delta notation, which is the permil deviation of the ratio of a heavy isotope to the most abundant isotope (^{32}S) in the sample compared to a standard ratio:

$$\delta^{x}S\,(‰) = \left[\frac{\left(\frac{n(^{x}S)}{n(^{32}S)}\right)_{sample}}{\left(\frac{n(^{x}S)}{n(^{32}S)}\right)_{V-CDT}} - 1\right] \times 1000 \quad (1)$$

where n is the number of atoms, ^{x}S is one of the heavy isotopes, ^{33}S, ^{34}S or ^{36}S, and V-CDT is the international sulfur isotope standard, Vienna Canyon Diablo Troilite, which has isotopic ratios of $^{34}S/^{32}S = 0.044163$ and $^{33}S/^{32}S = 0.007877$ (Ding et al., 2001). Isotopic fractionation is represented by the α value, which is the ratio of the heavy to the light isotope in the products divided by the ratio in the reactants:

$$\alpha_{34} = \frac{\left(\frac{n(^{34}S)}{n(^{32}S)}\right)_{products}}{\left(\frac{n(^{34}S)}{n(^{32}S)}\right)_{reactants}} \quad (2)$$

Values of α_{34} are characteristic for different reaction pathways and are therefore useful to investigate the different oxidation pathways for SO_2 on mineral dust in the laboratory and in the atmosphere.

This study presents measurements of the stable isotope fractionation of $^{34}S/^{32}S$ at room temperature (19 °C) during heterogeneous oxidation on dust surfaces and aqueous oxidation in dust leachate. The dust used is from the Sahara desert, which accounts for ~60 % of global dust emissions and loading (Tanaka and Chiba, 2006). The dust was collected on the Cape Verde islands (SDCV), and its mineralogy, composition and properties, as well as details on collection, are described in

ACPD
12, 2303–2353, 2012

Coude-Gaussen et al. (1994) and Hanisch and Crowley (2001, 2003). We demonstrate that stable sulfur isotopes can be used to understand SO_2 oxidation on mineral dust both in the laboratory and in the field, and are particularly useful to investigate the roles of different minerals in surface oxidation and to quantify the importance of aqueous oxidation by transition metal ions in the atmosphere.

2 Background: uptake and oxidation of SO_2 by mineral dust

Uptake of SO_2 to mineral dust can occur via the reversible, physisorption pathway, or the irreversible, chemisorption pathway, which can be followed by oxidation of the sorbed sulfite. This study will only consider irreversible uptake, which can account for $>98\,\%$ of uptake at low SO_2 concentrations (Adams et al., 2005; Goodman et al., 2001). The initial uptake coefficient on Sahara dust, $\gamma = 4 \times 10^{-5}$, is not dependent on RH, $[SO_2]$ or O_3 (Crowley et al., 2010) which suggests SO_2 adsorption is the rate-limiting step, rather than subsequent reactions and oxidation (Ullerstam et al., 2002).

Oxidation of adsorbed S(IV) can follow a number of pathways: O_3 is a very efficient oxidant, and oxidation can also be catalysed by iron and manganese in dust (Usher et al., 2002; Ullerstam et al., 2002). NO_2 (g) and surface nitrate have been observed to oxidise surface sulfite (Ullerstam et al., 2003), and oxidation to $CaSO_4$ occurs when calcite is exposed to SO_2 and O_2 (Al-Hosney and Grassian, 2005). Sulfate production has even been observed on MgO in the absence of O_2 and O_3, and was attributed to the highly basic character of four-coordinated O anions on steps and corners (Pacchioni et al., 1994; Goodman et al., 2001). In this study, SO_2 will always be exposed to dust in synthetic air, and the reaction time will be very long, so the oxidation of adsorbed sulfite to sulfate should be close to completion (Ullerstam et al., 2002).

The SO_2 removal rate on dry dust decreases significantly with exposure to SO_2 as saturation is approached, suggesting uptake will only be important for ~ 10 h after dust emission (Judeikis et al., 1978). However, active sites can be regenerated by exposure to high humidity for a number of reasons, for example carbonic acid dissociation

ACPD
12, 2303–2353, 2012

and release as CO_2 (g), increased mobility of surface ions leading to microcrystallite formation, and direct generation of new active sites (Ullerstam et al., 2002, 2003; Al-Hosney and Grassian, 2005; Li et al., 2006). IR absorption bands for adsorbed sulfate do not change upon exposure to humidity (Ullerstam et al., 2002, 2003). Saturation behaviour of SO_2 under exposure to UV light has not been measured, however irradiation prevents surface saturation for ozone uptake on TiO_2 (Nicolas et al., 2009). These results suggest that experimental conditions such as humidity, ozone and irradiation will change the quantity of SO_2 taken up and oxidised, while the initial uptake to form sorbed S(IV) is the rate-limiting step and is therefore expected to be the major factor controlling isotopic fractionation.

Aqueous oxidation by ions leached from dust may be a particularly important contributor to oxidation of SO_2 in the atmosphere, especially as sulfate production increases aerosol hygroscopicity and CCN activity, facilitating further aqueous SO_2 oxidation (Usher et al., 2002; Ullerstam et al., 2002, 2003; Li et al., 2006). The oxidative activity of leachates is due to catalysis by metal ions: Fe(III) is the most important of these ions, however comparison to experiments with pure Fe salts show trace ions such as Mn and Cr also make a significant contribution to catalytic activity (Tilly et al., 1991; Rani et al., 1992). Catalytic activity does not significantly change when the solid phase is filtered out of the leachate. This shows aqueous oxidation dominates over any surface effects of particles in the solution (Cohen et al., 1981; Rani et al., 1992), although, when aqueous iron and titanium oxide suspensions are irradiated, sulfate quantum yields $\gg 1$ have been observed due to desorption of $\cdot SO_3^-$ and initiation of a radical chain reaction (Hong et al., 1987; Faust et al., 1989).

Aqueous oxidation shows complex pH-dependence, as metal ions are more soluble but the more reactive SO_3^{2-} is less abundant at lower pH (Cohen et al., 1981; Rani et al., 1992). Dust is not the only contributor of transition metal ions for SO_2 oxidation: transition metals ions from anthropogenic sources are generally more soluble than ions in dust, and thus more available for reaction with S(IV) in solution (Kumar et al., 2010). The reaction pathways catalysed by anthropogenic and natural transition metal ions are

ACPD
12, 2303–2353, 2012

the same once the ions are leached into solution, thus the fractionation factor measured for dust leachate in this paper will also be applicable to leachate from combustion products such as fly ash (Cohen et al., 1981).

3 Methods

3.1 Apparatus and experiments

The dust used in this study was Sahara dust collected from the Cape Verde islands (SDVC). Its mineralogy, composition and properties are described in Coude-Gaussen et al. (1994) and Hanisch and Crowley (2001, 2003) and summarised in Table 1. The non-clay fraction of the dust contains primarily quartz, feldspars and calcite. Sahara sand obtained directly from the Sahara desert has a mean diameter of $>150\,\mu m$ (Morales, 1986), whereas transported dust contains dust particles as small as 200 nm and has a mean diameter of $<10\,\mu m$ that decreases with distance transported (Heinold et al., 2009; Kaaden et al., 2009; Wagner et al., 2009; Morales, 1986). Thus, Sahara dust from the Cape Verde Islands is much more relevant to atmospheric chemistry than a local sand sample which would include very coarse grain sizes.

3.1.1 Aqueous oxidation in mineral dust leachate

Leachate representing 0.5 g of dust per 100 ml was prepared by soaking the dust for two days in MilliQ water. The liquid phase was then poured off the solid dust as aqueous oxidation has been shown not to be affected when the solid phase is removed (Cohen et al., 1981; Rani et al., 1992). The concentrations of Al, Ca, Fe, Mg, Ba, Mn, Ti, Cr and Sr in the leachate were measured by inductively-coupled plasma optical emission spectrometry with a Perkin-Elmer Optima 3300 XL. SO_2 gas (Linde AG, 102 ppm ± 2 % in synthetic air) was diluted with synthetic air (Westfalen AG, 20.5 % O_2 in N_2) to 6.7 ppm and 13.3 ppm in a total flow of 600 sccm for experimental runs #1 and

ACPD
12, 2303–2353, 2012

#2, respectively. This flow was passed through 300 ml of leachate in a bubbler, followed by a bubbler containing 6 % H_2O_2 to collect residual SO_2 as described in Harris et al. (2012). PFA fittings and tubings were used for all gas flows. The experiments were run for ~ 8 h. Following each experiment, both bubblers were rinsed and $BaCl_2$ was added to precipitate sulfate as $BaSO_4$. The $BaSO_4$ was collected by filtration through Nuclepore track-etch polycarbonate membrane filters (Whatman Ltd.) with 0.2 µm pores, which had been coated with a 10 nm-thick gold layer using a sputter coater (Bal-tec GmbH, Model SCD-050) prior to sample collection.

3.1.2 Heterogeneous oxidation on the Sahara dust surface at subsaturated humidity

Heterogeneous oxidation on mineral dust was investigated by passing 250 sccm of 4.2 ppm SO_2 gas in synthetic air through a dust-coated filter, as shown in Fig. 1. Dust was pipetted on to gold-coated Nuclepore filters (0.2 µm pore) in a 1 : 2 ethanol : water mixture, which helped the dust to adhere to the filter better than mounting in pure water. A mixed cellulose ester filter (Whatman GmbH) was placed under the Nuclepore filter to prevent tearing when gas flows were switched on and off. The mounted dust had a modal diameter of 2 µm with maximum grain diameters of ~ 8 µm, showing the dust was not significantly size-fractionated during mounting compared to the results of Coude-Gaussen et al. (1994). The reactor was made of glass with an FEP O-ring (Ralicks Industrie- und Umwelttechnik) connecting the two parts. PFA fittings and tubings were used for gas flows. SO_2 gas (Linde AG, 102 ppm ± 2 % in synthetic air) was diluted with synthetic air (Westfalen AG, 20.5 % O_2 in N_2) to the desired concentration before entering the reactor. A high concentration of SO_2 (4.2 ppm) was used to prevent significant isotopic changes to the residual SO_2. Less than 1 % of the SO_2 gas reacted to form sulfate in all experiments. The residual SO_2 gas was collected in some experimental runs as described in Harris et al. (2012) and the isotopic composition confirmed the SO_2 was not significantly altered during the experiments.

ACPD
12, 2303–2353, 2012

The reaction system was run under a variety of different conditions, which are summarised in Table 2 along with abbreviations that will be used throughout this paper. A high power LED ($\lambda_{max} = 365$ nm, 50 mW at 350 mA, Roithner Lasertechnik GmbH) was used to irradiate the dust in four experiments through a Suprasil quartz window (Heraeus Quarzglas GmbH), which has a transmittance of > 90 % between 200 and 1000 nm. The emission spectrum of the LED is shown in Fig. 2, along with the absorption spectra of O_3 and SO_2. Neither O_3 or SO_2 absorb significantly in the wavelength range of the LED, so no gas-phase photolytic reactions will occur. Humidity was added to the reaction chamber in four experiments by passing the synthetic air flow through MilliQ water to achieve a relative humidity of around 40 %, which would correspond to 2 monolayers of water on the dust (Gustafsson et al., 2005). The dust was not heated before use, so even samples with no added humidity will have surface-sorbed water molecules and inter-lamella water in the clay fraction. 20 ppm ozone was added to the gas mixture in four experiments by passing 100 sccm of the synthetic air flow over a low-pressure mercury vapour lamp (Jelight Company Inc., USA). The ozone concentration was measured with a Thermo Electron Corporation UV Photometric O_3 Analyzer (Model 49C). Each experiment was done in duplicate with and without the addition of humidity, for a total of 16 experimental runs. The experiments were run for 6–9 h to generate sufficient sulfate for NanoSIMS isotopic analysis. Following each experiment, filters were stored in airtight boxes before being mounted for NanoSIMS and SEM analysis.

3.2 SEM analysis

A scanning electron microscope (SEM) was used to investigate the quantity of sulfate produced during the leachate experiments and the composition of individual dust grains in the different samples for the surface reaction experiments. The $BaSO_4$ and dust samples on gold-coated filters were directly analysed in the SEM without any further treatment. A LEO 1530 field emission SEM with an Oxford Instruments ultra-thin-window energy-dispersive X-ray detector (EDX) was used for the analyses. The SEM

ACPD
12, 2303–2353, 2012

was operated with an accelerating voltage of 10 keV, a 60 µm aperture and a working distance of 9.6 mm. "High current mode" was used to increase the EDX signal and improve elemental sensitivity.

Before NanoSIMS analysis of the samples, the SEM was run in automatic mode and took 400 evenly-spaced images of each filter at 19 500 × magnification. The EDX spectrum was measured with a 1 s integration time at 25 points on a 5 × 5 grid for each image, leading to 10 000 EDX measurements across each filter. For the leachate oxidation $BaSO_4$ samples, EDX signals were measured for $O(K_\alpha)$, $Au(L_\alpha)$, $S(K_\alpha)$ and $Ba(L_\alpha)$. The quantity of sulfate on each filter was then determined by estimating the background from both the Gaussian distribution of the gold signal and the quartile method, as described in Harris et al. (2012) and Winterholler (2007). This quantification method is ideal for NanoSIMS studies, as quantification is achieved without extra sample treatment and the limit of detection is very low. The precision is fairly low (∼ 40 %, decreasing with increasing $BaSO_4$ quantity due to Poisson statistics) and the method is not ideal for samples with a large amount of $BaSO_4$ due to the possibility of the sample flaking off the filter during mounting, thus isotope mass balance was also used to find the extent of reaction (see Sect. 4.1), as was used in Lin et al. (2011), Harris et al. (2012) and Derda et al. (2007).

During the analyses of the dust grains from the surface oxidation experiments, seven EDX channels were measured in automatic mode: $Fe(L_\alpha)$, $Mg(K_\alpha)$, $Al(K_\alpha)$, $Si(K_\alpha)$, $S(K_\alpha)$, $Ca(K_\alpha)$ and $Ti(K_\alpha)$. The background was subtracted from the signals using the quartile method (Harris et al., 2012; Winterholler, 2007). The signals were used to investigate the composition of the mineral dust and association of sulfate with the different elements in the dust. The SEM images were also used to measure the size distribution of the dust, as described in Winterholler (2007). The density of the dust was estimated to be 3.1 g cm^{-3} from the densities of the three main components, SiO_2, Al_2O_3 and FeO, and this was used to calculate the mass of dust on each filter. The BET surface area of the dust was measured by Hanisch and Crowley (2001) to be 1.5 m^2 g^{-1} for grains with $d < 10$ µm.

ACPD
12, 2303–2353, 2012

Following NanoSIMS analysis, the dust grains from the surface oxidation experiments were again examined in the SEM, to determine the chemical composition of the dust grain for each NanoSIMS analysis point. Coordinate transfer was used to locate the grains in the SEM and an image and an EDX spectrum were then taken at each point. An example is shown in Fig. 3. Peaks were counted if they were more than three times the noise at the peak position (Goldstein et al., 1981), and an approximate height was measured by overlaying a grid as shown in the figure. The known composition of the dust (Hanisch and Crowley, 2003) was used to determine relative sensitivity factors (RSF) for the different elements based on the EDX measurements on unreacted dust grains. RSF values were in the expected range of 0.1 to 2 (Goldstein et al., 1981). An approximate atomic percentage for all detectable elements could then be estimated for each experimental grain. The error in atomic percentage was defined as ± 1 unit on the overlayed scale, multiplied by the RSF for the element. The resulting composition obtained for each dust grain is not surface-sensitive as the X-rays are released from a depth of < 1 µm (Goldstein et al., 1981), so the results will show the elements present at the analysis point but will not be especially sensitive to the newly-produced sulfate from the experimental treatment.

3.3 NanoSIMS analysis

The sulfur isotopic composition was determined with the Cameca NanoSIMS 50 ion probe at the Max Planck Institute for Chemistry in Mainz (Hoppe, 2006; Groener and Hoppe, 2006). The NanoSIMS 50 has high lateral resolution (< 100 nm) and high sensitivity and can simultaneously measure up to five different masses through a multicollection system, allowing high precision analysis of the small sample quantities required for this study. The use of this instrument to analyse sulfur isotope ratios is described in detail elsewhere (Winterholler et al., 2006, 2008) and the analysis conditions are described in Harris et al. (2012), so only a brief description will be given here.

The samples are analysed directly on the gold-coated Nuclepore filters without further processing. Samples with a particularly high $BaSO_4$ loading and all dust samples are gold-coated on top of the sample before NanoSIMS analysis to prevent excessive

ACPD
12, 2303–2353, 2012

charging. A ∼ 1 pA Cs^+ beam is focussed onto a ∼ 100 nm sized spot and rastered in a 2 µm × 2 µm grid over the grain of interest. The ejected secondary ions are carried into the mass spectrometer and multicollection system. For the $BaSO_4$ from leachate oxidation experiments, each measurement consists of 200–400 cycles of 4.096 s duration preceded by varying lengths of presputtering until the gold coating (if present) is removed and the count rate is stable. For the surface oxidation samples, the sulfate produced in the experiments will be on the surface of the particles, so analyses were fairly short and presputtering was kept to a minimum: each measurement consisted of 120 cycles of 4.096 s duration, and presputtering and beam centering were carried out on an area of at least 10 µm × 10 µm so that the surface was conserved for analysis.

The session instrumental mass fractionation (IMF) was determined with IAEA $BaSO_4$ standards SO5 and SO6, however the IMF for sulfate on mineral dust grains will also be dependent on the matrix. The major cation was determined from SEM-EDX analysis taken on individual grains after the NanoSIMS analysis, as described in the previous section, and the IMF correction relative to $BaSO_4$ was then applied according to Winterholler et al. (2008). The untreated Sahara dust contained a measureable quantity of sulfate, so a background correction of the isotope ratio was needed for the surface oxidation samples. The effect of this was minimised by keeping analyses short so that primarily surface sulfate was analysed, however the background was still significant. 28 untreated grains were analysed to quantify the background sulfur isotope signal. The untreated grains had an average ^{32}S signal of 447 ± 385 counts per second and a $\delta^{34}S$ of 18.6 ± 5.9 ‰. This falls within the range of values previously reported for sediments in the Sahara desert (Drake et al., 2004) and Sahara dust collected in the North Atlantic (Winterholler et al., 2006). Thus, experimentally-treated grains were only considered in the data analysis if their ^{32}S signal was > 900 counts s^{-1}, and values of $\delta^{34}S$ for these grains were corrected for the isotopic composition of the background. 102 experimental grains had high enough ^{32}S counts for useful isotopic information, and these were distributed fairly evenly across the different experiments, so that at least eight grains per sample gave useful information for each set of experimental conditions.

ACPD
12, 2303–2353, 2012

For each sample of the leachate experiments, at least five spots were measured and the weighted average and error was calculated, as described in Harris et al. (2012). The counting statistical error was typically 1–2 ‰ for each analysis spot and the overall error for each sample 2–5 ‰. For the surface oxidation experiments, the spot-to-spot error was added to the counting statistical error so that the measurements on each grain could be treated individually, rather than calculating an average for all grains on a particular sample filter. The spot-to-spot error of the SO5 and SO6 standards was used as an estimate of the spot-to-spot error for the measurement session, and this was then combined with the counting statistical error to determine the measurement uncertainty for each individual grain. For each individual grain, the counting statistical error was typically 4–5 ‰ and the overall error 5–6 ‰.

3.4 Positive matrix factorization

The composition of each grain from post-NanoSIMS SEM analysis was used as input for a Positive Matrix Factorization (PMF) model which was run with the software EPA PMF v3.0.2.2. This is a multivariate analysis tool which identifies factor profiles and factor contributions for data sets which have a large number of variables measured across many samples (Norris et al., 2008). Although the model is designed to identify source profiles and contributions to environmental data sets, it is ideal for this study as it allows data points to be individually weighted and it constrains results so that no factor can have a negative contribution to a sample.

Atomic percentages of O, Fe, Na, Mg, Al, Si, S, K, Ca and Ti were used as input for the model, as well as S isotope measurements from NanoSIMS analysis. When a peak was below the limit of detection, an atomic percentage of one third of the lowest measured concentration for the element was used, and the uncertainty was set to twice the normal uncertainty for the element to reduce the weighting of the point. All elements were classed as "strong" as the uncertainties did not need to be increased, however $\delta^{33}S$ was classified as a "weak" variable as its analysis in the NanoSIMS can be problematic due to counting statistics combined with topography and matrix effects.

ACPD
12, 2303–2353, 2012

$\delta^{34}S$ was set as the "total variable", leading to an automatic "weak" classification. The "Extra Modeling Uncertainty" was set to the recommended 5 % (Norris et al., 2008). No two elements showed any significant correlation.

A random seed was used to initiate the model and 20 base runs were performed. The model was run with three, four and five factors and it was found that four factors gave the most consistent results with the lowest Q (object function) value and the best resolution of elements and isotopic compositions. Only the four factor analysis will be discussed further. The model described the data adequately: the residuals were approximately normally distributed and only one scaled residual for one Al value was outside the $\pm 3\sigma$ limit. The overall profiles of the four identified factors varied only a small amount between the 20 model runs, and the dominant species in each factor remained the same in all 20 runs.

4 Aqueous oxidation in Sahara dust leachate

4.1 Catalytic activity of the solution and rate of reaction

The concentrations of various elements present in the leachate, measured with ICP-OES, are shown in Table 3. The leachate was extremely efficient at oxidising SO_2, thus the fractionation factor must be found by considering the Rayleigh equations, which describe the isotopic composition of products and residual reactants as a function of the fractionation factor and the fraction of reactant remaining unreacted (Mariotti et al., 1981; Krouse and Grinenko, 1991). The fraction of SO_2 remaining was measured for each of the two experimental runs both with SEM quantification as described in Sect. 3.2 and by considering mass balance between the measured isotopic composition of the residual SO_2 and the product sulfate:

$$\delta^{34}S_i = f \cdot \delta^{34}S_{SO_2} + (1-f) \cdot \delta^{34}S_{sulfate} \quad (3)$$

ACPD
12, 2303–2353, 2012

where f is the fraction of reactant (SO_2) remaining and $\delta^{34}S_i$, $\delta^{34}S_{SO_2}$ and $\delta^{34}S_{sulfate}$ are the isotopic compositions of the initial SO_2 gas, residual SO_2 gas and product sulfate, respectively. For each experimental run both estimates differed by < 1 %, and the two estimates were averaged to find the fraction remaining for each of the experimental runs.

The oxidation of SO_2 by mineral dust leachate was very efficient. > 99 % of SO_2 was oxidised after passing through one bubbler, compared to the 39 % of SO_2 that is collected in one bubbler containing 6 % H_2O_2 and < 1 % that is oxidised in a bubbler with 0.1 M Fe^{2+}/Fe^{3+} (Harris et al., 2012). The fraction oxidised at $[SO_2] = 6.7$ ppm (99.8 %) was only slightly higher than the fraction oxidised at $[SO_2] = 13.3$ ppm (99 %), showing the leachate was not close to exhausting its oxidation capacity. Thus, it is clear iron is not the most important transition metal for the catalysis of SO_2 oxidation in mineral dust leachate solutions; other ions measured in the solution, such as manganese and chromium, are also highly active in oxidation. This is in agreement with the results of Tilly et al. (1991) and Rani et al. (1992), which showed that these ions do not just contribute independently to oxidation, but that mixtures of ions interact synergistically, resulting in greatly-enhanced oxidation rates. Thus, soluble iron alone is not a good indicator of SO_2 oxidising ability, which may explain why correlation between soluble Fe and sulfate is often poor (Kumar and Sarin, 2010; Baker et al., 2006).

4.2 Fractionation of $^{34}S/^{32}S$ during aqueous oxidation in Sahara dust leachate

The fractionation factor can be found from the Rayleigh equation describing the $\delta^{34}S$ of the sulfate product with respect to the fraction of SO_2 oxidised (Mariotti et al., 1981; Krouse and Grinenko, 1991):

$$\alpha_{34} = \frac{\ln\left(1 - \left(\frac{R_p}{R_i}\right)(1-f)\right)}{\ln f} \quad (4)$$

ACPD
12, 2303–2353, 2012

where R_p and R_i are the ratios of $^{34}S/^{32}S$ for the product sulfate and the initial SO_2 gas, respectively and f is the fraction of SO_2 remaining. The $\delta^{34}S$ of the sulfate formed in the leachate needs to be corrected for the contribution from sulfate that was leached from the dust itself. The effect of this correction on $\delta^{34}S_p$ was negligible as the leachate contained < 1 µM of sulfate while the reaction added > 200 µM of sulfate to the solution.

The fractionation factor can also be found from the Rayleigh equation describing the $\delta^{34}S$ of the residual SO_2 gas and the fraction of SO_2 oxidised (Mariotti et al., 1981; Krouse and Grinenko, 1991):

$$\alpha_{34} = \frac{\ln\left(\frac{R_r}{R_i}\right)}{\ln f} - 1 \quad (5)$$

where R_r and R_i are the ratios of $^{34}S/^{32}S$ for the residual SO_2 gas and the initial SO_2 gas, respectively and f is the fraction of SO_2 remaining. The measured $\delta^{34}S$ of the residual SO_2 was corrected for fractionation during collection in H_2O_2 as described in Harris et al. (2012).

Four estimates of α_{34} were thus obtained: from the residual SO_2 and the product sulfate for each of the two experimental runs. The four measurements were averaged and the 1σ standard deviation taken as the error:

$$\alpha_{\text{leachate}} = 0.9917 \pm 0.0046 \quad (6)$$

at 19 °C. The majority of the uncertainty in the fractionation factor is due to the uncertainty in the NanoSIMS measurements of the $\delta^{34}S$ values. The fractionation factor is not significantly different to the fractionation factor for the oxidation of SO_2 by a solution of Fe^{2+} and Fe^{3+} ($\alpha_{Fe} = 0.9894 \pm 0.0043$) measured by Harris et al. (2012). However, in agreement with previous studies (Cohen et al., 1981; Tilly et al., 1991; Rani et al., 1992), the quantity of sulfate produced (see Sect. 4.1) shows that iron is not the only transition metal present in leachate that is active in catalysing SO_2 oxidation. Concentrations of other transition metals in the leachate that are also available for reaction,

ACPD
12, 2303–2353, 2012

such as Cr and Mn, are presented in Table 3. Thus, the identity of the metal catalysing SO_2 oxidation does not affect the sulfur isotope fractionation, which suggests fractionation is not due to the initiation reaction but the subsequent reactions in the chain (Herrmann et al., 2000). The average fractionation factor for transition metal-catalysed oxidation of SO_2 from the current and previous measurements is:

$$\alpha_{TMI} = 0.9905 \pm 0.0031 \quad (7)$$

5 Fractionation of $^{34}S/^{32}S$ during heterogeneous oxidation on Sahara dust surfaces

5.1 Quantification of sulfate production

Sulfate production on the dust surface and subsaturated humidity was quantified as described in Sect. 3.2, and the results are shown in Fig. 4. Experiment lengths ranged from 6.3 to 9.2 h, so the results shown were corrected and represent the estimated concentration after exactly 8 h of experimental time, to factilitate comparison between experiments. The surface sulfate increase will be significantly more than the reported total atomic percentage increase, as EDX measurements are not surface-sensitive (Goldstein et al., 1981). As an estimate, for a grain 2 µm in diameter with experimentally-produced sulfate added only to the top 20 nm of the grain surface, the sulfate concentration in the surface layer would increase by more than 1000 % for MDRHO3hv, rather than the 30 % increase when the whole grain volume is considered. The total amount of sulfate was seen to increase in all experiments except for MDRHhv, although all changes are within the statistical error of the SEM measurement except for MDRHO3hv. The count rates observed during NanoSIMS analysis show an increase for all treated samples compared to the control, and are also much higher for MDRHO3hv, in agreement with the SEM samples. Thus, sulfate production is fairly slow and similar for all experiments except MDRHO3hv: this combination of conditions saw much more sulfate produced than the other experiments combined, showing

ACPD
12, 2303–2353, 2012

ozone, light and water vapour interacted synergistically to oxidise SO_2 much more efficiently than any of these parameters alone.

5.2 Bulk elemental analysis of reactive particles

Correlations between the sulfur EDX signal and the EDX signal of other elements may provide information on which elements are most important for sulfate production. Automatic EDX points with sulfur and at least one other element above the background were therefore examined for correlations, in both the untreated and treated dust samples. Each sample had > 100 EDX points with significant signals for sulfate and at least one other element, so correlations could be examined individually within each sample type. In untreated dust, correlations can indicate whether the sulfate present is primary and present in the Sahara source region, or whether it is secondary and results from uptake and reactions during transport to the Cape Verde Islands. S and Ti signals show a slight positive correlation ($R^2 = 0.35$) in the untreated samples, which suggests the sulfate is secondary: primary sulfate would be more likely to be associated with Ca and Mg due to clays and minerals such as gypsum (Caquineau et al., 2002).

Correlations on experimental samples were only seen for those runs with no ozone or irradiation: S on MDdark dust was weakly correlated with Ti and Fe ($R^2 = 0.19$ and 0.13, respectively), while S on MDRHdark dust was strongly correlated with Ti and Ca ($R^2 = 0.66$ and 0.53, respectively). No mineralogical information is provided in automatic EDX analysis, and it is likely that the lack of correlation in other samples is because element concentrations are a poor representation of element availability for reaction, rather than an indicator that sulfate is produced evenly across dust grains. The SEM-EDX analysis also has a resolution of only $\sim 1\,\mu m$, and grain heterogeneity with regards to mineralogy on this scale (Falkovich et al., 2001) will obscure correlations in the SEM-EDX signal.

Elements which are associated with higher SO_2 oxidation rates can also be examined by looking at the elemental profile of dust grains (from post-NanoSIMS single-particle SEM-EDX analysis) with high enough ^{32}S count rates for isotopic analysis,

ACPD
12, 2303–2353, 2012

compared to the overall dust profile. This comparison is shown in Fig. 5. It can be seen that Ti is strongly enriched in oxidising dust, and K, Fe and Ca are slightly enriched, while Na, Mg, Al, Si and O show no relationship to oxidising ability of dust and only fall slightly below the 1 : 1 line because of mass balance. This is consistent with the correlations from automatic SEM analysis: Ti, Fe and Ca are the most important elements for oxidising ability, particularly in dark experiments where ozone and light are not available to facilitate further reaction pathways, while mineralogy is clearly the dominant factor controlling uptake.

5.3 $^{34}S/^{32}S$ fractionation on different dust components

The isotopic composition of sulfate on experimentally-treated samples was much more variable than on control grains, even within one set of experimental conditions. Variability within one set of experimental conditions was as large as overall variability of the data set. As atmospheric dust is strongly internally mixed with regards to mineralogy (Falkovich et al., 2001) most analysed grains will represent a mix of minerals, so a multivariate analysis model (described in Sect. 3.4) was used to examine the relationship between grain composition and isotopic fractionation. Four factors were identified from the PMF analysis. Each factor is not representative of a single mineral, but rather of a group of minerals that, acting together or separately, cause the same isotopic fractionation during sulfate formation. The elemental profiles of these factors are shown in Fig. 6. To determine the isotopic fractionation factor of the factor, factor contributions for each grain were plotted against $\delta^{34}S$. The intercept where the factor contribution was one gave the fractionation factor α_{34} of the factor.

The factor α_{34} values were used to predict the $\delta^{34}S$ of the measured dust grains based on their composition, to test the fit between modelled and actual fractionation. The discrepancy between predicted and measured $\delta^{34}S$ was no greater than what would be expected from a normal distribution given the measurement error (Fig. 7), and the regression line weighted by the error in the measurements was ($R^2 = 0.62$):

ACPD
12, 2303–2353, 2012

$$\delta^{34}S_{observed} = (0.90 \pm 0.11)\delta^{34}S_{predicted} - (5.81 \pm 2.54) \quad (8)$$

which shows that the model fits the data well. However, this is not a rigorous test of the model as the same 102 measurements were used to generate the factor α_{34} values and to test them, but it indicates the factors are well-resolved with respect to isotopic fractionation.

Plots to determine fractionation factors were made for all samples together, as well as for sub-groups of samples to determine the role of experimental conditions in isotopic fractionation. The results are shown in Fig. 8. The error in the estimates of α_{34} for the sub-groups are much higher due to the much smaller number of measurements (47 and 55 grains for "all humid" and "all dry", respectively; 20–31 grains for the effects of O_3 and light). The α_{34} could not be determined for individual experimental conditions (eg. MDO3 or MDRHhv) as the number of grains (8–14) was too small, thus the uncertainty in the result too large to be useful. It can be seen that presence or absence of humidity, light and ozone has much less effect on the isotopic fractionation than the dust composition: fractionation factors for different subsets generally agree with overall fractionation within the error for each factor. This shows that isotopic fractionation is primarily due to uptake of SO_2 (g) and not subsequent oxidation.

Based on the elemental profile of each factor, its interaction with experimental conditions, and its reactivity, the mineralogical identity and reaction mechanism associated with each factor was inferred. They are discussed in the following sections and summarised in Table 4. Several estimates of the oxidation rate for each factor were obtained: the sulfate production percentage refers to the percentage of the total sulfate that was generated by that factor during the experiment. The reactivity ($\mu g\,sulfate\,g^{-1}\,mineral\,h^{-1}$) is the amount of sulfate produced per gram of the minerals represented by the factor, divided by length of the experiment; the calculation does not consider decreases in rate due to saturation of the dust surface, and it is assumed that the surface fractions of the minerals are the same as the bulk fractions. This rate is relevant for the length of the experiments (6–9 h), but will eventually decrease as the dust is saturated. The reactivity could be used to estimate the rate of SO_2 oxidation

ACPD
12, 2303–2353, 2012

and sulfate production on different dust types based on their mineral assemblages, however further investigation would be necessary given the strong role of mineral mixing in oxidation rate. The rate represented by the reactivity refers to the MDRHO3hv experiments, where the largest amount of sulfate was produced; oxidation under all other conditions is on average 16 × slower and the uncertainty is much greater.

The reactivity and the BET surface area were used to estimate the reactive uptake coefficient γ for the dust according to Jayne et al. (1990):

$$\gamma_{\text{obs}} = \frac{4F_{\text{g}}}{\bar{c}A}\frac{\Delta n}{n} \tag{9}$$

where F_{g} is the carrier gas flow rate ($\text{cm}^3\,\text{s}^{-1}$), $\bar{c}$ is the mean thermal velocity ($\text{cm}\,\text{s}^{-1}$; $\sqrt{\frac{3k_B\text{T}}{m}}$), A is the total droplet surface area (cm^2) and $\frac{\Delta n}{n}$ is the reduction in gas concentration. The γ_{obs} value found from this expression represents a combination of mass transfer, accommodation and reaction limitations, and provides only an estimate of the reactive uptake rate as it does not account for diffusion rate within the solid. The overall γ_{obs} for the dust, considering both reactive and non-reactive components, is 2.7×10^{-6}, which is ∼1 order of magnitude lower than previously reported values (Crowley et al., 2010). This is well within the expected range considering the surface area of the dust is likely to be overestimated in this study as the dust is lying on a filter, rather than suspended in a flow reactor, and the previously reported values are for initial uptake coefficients before uptake slows due to aging and saturation. The dust in this study is a good representation of atmospheric dust that has already been aged, as it was transported from the Sahara desert to the Cape Verde Islands before being collected for use in experiments.

5.3.1 Factor 1

Factor 1 has a fractionation factor of $\alpha_{34} = 1.012 \pm 0.010$ which shows no significant variation depending on experimental conditions. It has high concentrations of Fe and Ti (6.8 and 13.2 at. %, respectively) and the highest reactivity of any factor, which is

ACPD
12, 2303–2353, 2012

in agreement with observations of relatively high uptake coefficients for SO_2 on TiO_2 and on iron oxides and oxyhydroxides (Zhang et al., 2006; Crowley et al., 2010). The co-occurence of Fe and Ti suggests that the factor is representative of ilmenite, with some degree of weathering towards pseudorutile and rutile accounting for the excess Ti (Janssen et al., 2007; Putnis, 2002). Ilmenite is a chemically stable mineral that would be likely to have survived transport from the Sahara to the Cape Verde Islands and aging while on the Cape Verde Islands prior to collection (Janssen et al., 2007). The importance of Ti in the most reactive factor agrees with the EDX sulfur correlation results from Sect. 5.2 which found Ti to be enriched in areas where sulfate production was highest.

As the uptake of SO_2, rather than the oxidation, controls isotopic fractionation, the coordination mechanism for SO_2 should relate to the isotopic fractionation. Given that the α is robust to experimental conditions and well-resolved for Factor 1, the fractionation factor on the rutile (TiO_2) and on the parent ilmenite are the same. Hematite, goethite, magnetite and TiO_2 have all been shown to chemisorb SO_2 to a bidentate complex, with similar IR spectral bands observed for the adsorbed compounds where available. This suggests these three iron oxides will also have the same value for α as TiO_2 and by extension the same α as ilmenite (Fu et al., 2007; Zhang et al., 2006; Usher et al., 2002). Factor 1 also has a significant amount of Ca. This may be due to formation of $CaSO_4$ from colocated Ca^{2+}, possibly as the sample dries when it is put under vacuum for analysis. It is unlikely that CaO or $CaCO_3$ are directly taking up sulfate as the mechanisms of uptake (monodentate and direct reaction, respectively) are very different to iron and titanium oxides, and would not be expected to show the same fractionation factor (Usher et al., 2002).

In summary, ilmenite and its weathering product rutile are the most active components in SO_2 uptake in Sahara dust, and chemisorb SO_2 to a bidentate complex with a fractionation factor of $\alpha_{34} = 1.012 \pm 0.010$, which is expected to also represent fractionation on hematite, goethite and magnetite. Sulfate production was calculated to be 12.64 µg per mg of iron and titanium oxides and their weathering products per hour.

ACPD
12, 2303–2353, 2012

5.3.2 Factor 2

Factor 2 contributes 3.2 % of total sulfate production, and produces sulfate that is strongly enriched in ^{32}S. The elemental composition suggests the factor represents feldspar, which is known to be a common constituent of Sahara dust (Coude-Gaussen et al., 1994; Glaccum and Prospero, 1980). Al_2O_3 alone can have a relatively high uptake coefficient if it is basic in character (Judeikis et al., 1978; Crowley et al., 2010), while SiO_2 and acidic Al_2O_3 have very low uptake coefficients (Zhang et al., 2006). Adsorption at acidic sites is reversible physisorption, while irreversible chemisorption occurs at basic sites and can be followed by oxidation (Karge and Dalla Lana, 1984). Thus, uptake in this factor will be dominated by basic sites associated with Al. Fe ions associated with the feldspar, and seen in the factor elemental composition, would increase the acidic character, consistent with the relatively low reactivity. Although Fe^{3+} can catalyse S(IV) oxidation (Herrmann et al., 2000), this reaction pathway will be insignificant without an aqueous phase.

The adsorption of SO_2 on Lewis base sites in Al_2O_3 results in sulfite with significantly different IR absorption bands to, for example, MgO (Goodman et al., 2001), which explains the strongly negative isotope fractionation that is very distinct from the other factors. The mechanism of uptake on to Al_2O_3 is coordination to exposed oxygen atoms (Lewis base sites) followed by rearrangement resulting in sulfite chemisorbed to aluminium through the sulfur atom.

In summary, basic aluminium oxide sites associated with feldspars, a common constituent of Sahara dust, chemisorb SO_2 with a fractionation factor of $\alpha_{34} = 0.948 \pm 0.012$, which is also expected to be the fractionation factor for adsorption on to pure basic aluminium oxides. The sulfate production due to this factor is 0.40 µg of sulfate per mg of feldspar and aluminium oxide per hour.

ACPD
12, 2303–2353, 2012

5.3.3 Factor 3

The isotope fractionation produced by Factor 3 was slightly positive and very similar to Factor 1. The contribution of Factor 3 to total sulfate formation was minor (0.1 %). The elemental composition of Factor 3 shows that it is primarily composed of quartz, as well as olivine and pyroxene, which are expected to be major components in Sahara dust (Coude-Gaussen et al., 1994; Glaccum and Prospero, 1980). However, pure SiO_2 has been measured to have very low or no reactivity with SO_2 (g) in the laboratory (Zhang et al., 2006; Usher et al., 2002, respectively). Li et al. (2007) found that the addition of MgO to NaCl resulted in an increase in reactivity towards SO_2 larger than that expected from the individual uptake coefficients, and Zhang et al. (2006) also found excess reactivity in a mixture of continental crust components such as SiO_2 and MgO. Factor 3 contains a significant amount of Mg as well as other cations so it is likely mixing of SiO_2 and components with basic character, such as magnesium oxides or olivine, has increased the reactivity of the quartz fraction of the dust to a significant level. Spectra and adsorption mechanisms for SO_2 on silicates are not available, but the similarity of the fractionation factor for Factor 3 to that of Factor 1 suggests a similar, but much slower, adsorption mechanism.

In summary, adsorption of SO_2 to mixtures of quartz and components with basic character results in a fractionation factor of $\alpha_{34} = 1.007 \pm 0.011$. The total sulfate production is 0.05 µg of sulfate per mg of quartz per hour.

5.3.4 Factor 4

Factor 4 contributes 11.7 % to the total sulfate production and produces sulfate strongly enriched in ^{34}S. The elemental profile shows that the factor represents clays, particularly smectite, illite and chlorite, which have been shown to be major components of the clay fraction of Sahara dust from the Cape Verde Islands (Coude-Gaussen et al., 1994). Interlayer cations such as Mg^{2+}, Ca^{2+} and Na^{+} are likely to be the components most available for reaction with SO_2, which is consistent with the correlation between Ca and

ACPD
12, 2303–2353, 2012

sulfate presented in Sect. 5.2. Uptake of SO_2 by MgO and CaO has a relatively high rate (Crowley et al., 2010; Usher et al., 2002; Zhang et al., 2006), however DRIFTS IR absorption bands for sorbed S(IV) suggest sulfite is adsorbed quite differently on CaO and MgO (Low et al., 1971; Goodsel et al., 1972) so it is unlikely the adsorption to interlayer cations in clays can be represented by adsorption to oxides. SO_2 will react directly with $CaCO_3$ to produce $CaSO_3$ which is readily oxidised to $CaSO_4$ (Al-Hosney and Grassian, 2005; Li et al., 2006), and an analogous reaction with interlayer Ca and Mg is most likely the cause of SO_2 uptake in Factor 4. Factor 4 also has a large amount of Ti, however the fractionation factor is not in agreement with Ti uptake from Factor 1. The calculated α_{34} for Factor 4 is lower, i.e. closer to the α_{34} of Factor 1, when the dust is exposed to O_3 or light, thus it appears that Ti associated with clay can only significantly contribute to SO_2 oxidation when the reaction is facilitated by light or O_3.

In summary, adsorption of SO_2 to interlayer cations, particularly Ca^{2+} and Mg^{2+}, in clays such as smectite results in a strongly positive fractionation of $\alpha_{34} = 1.085 \pm 0.013$. Sulfate production is 2.91 µg per mg of clay minerals per hour of reaction time.

5.4 Overall $^{34}S/^{32}S$ fractionation on Sahara dust

The total average fractionation factor for heterogeneous SO_2 oxidation on the surface of Sahara dust can be estimated by two methods. The weighted average of all 102 individual NanoSIMS measurements results in a $\delta^{34}S$ of 9.5 ± 3.9 ‰. The average composition from the PMF, found by weighting the α_{34} values from the different factors by their uptake efficiency and contribution to the total dust mass, is $\delta^{34}S = 10.1 \pm 9.9$ ‰. The two values agree very well and can be combined to estimate the average fractionation for the heterogeneous oxidation of SO_2 on the surface of Sahara dust:

$$\alpha_{het} = 1.0096 \pm 0.0036 \quad (10)$$

This average fractionation factor is only relevant for the particular dust sample measured in this study. The sulfur isotope fractionation factor for different dust sources

ACPD
12, 2303–2353, 2012

should be calculated based on the factor-specific fractionation factors and the mineralogy and ageing of the dust of interest.

5.5 Sensitivity of sulfate production and isotopic fractionation to O_3, light and humidity

As discussed in the preceeding sections, isotopic fractionation shows little sensitivity to the parameters that were varied between experiments. The relative contributions of the four factors to sulfate production were also not significantly affected by the experimental conditions. This shows chemical composition and mineralogy of a dust grain are the most important parameters causing differences in isotopic fractionation, with the experimental conditions playing a secondary role. Isotopic fractionation will be controlled by the rate-limiting step, as the fraction reacted for other reaction steps will be ~ 1, meaning that isotopic selectivity in these steps will not have an effect on the final product. The various experimental parameters would be likely to affect oxidation of adsorbed S(IV) but have less effect on initial uptake (Judeikis et al., 1978; Adams et al., 2005), thus the results of this study are consistent with previous laboratory studies, which have determined that SO_2 adsorption is the rate-limiting step for SO_2 uptake and oxidation on mineral dust (Ullerstam et al., 2002; Li et al., 2006).

The experimental parameters will affect the saturation behaviour of the dust, however in most experiments the oxidation rate was low and the dust was not exposed to SO_2 long enough to reach saturation (Mamane and Gottlieb, 1989). However, when the dust is exposed to humidity, light and ozone simultaneously (MDRHO3hv), the quantity of sulfate produced is >7 times higher than in any other experiment. Humidity regenerates the reactive capacity of dust for SO_2 uptake (Judeikis et al., 1978; Ullerstam et al., 2002), possibly due to the increased mobility of surface ions which leads to the re-exposure of active sites (Al-Hosney and Grassian, 2005). Uptake and decomposition of ozone, which increases the basicity and oxidising capacity of the surface, is highest when irradiated and at around $\sim 35\,\%$ RH (Hanisch and Crowley, 2003; Nicolas et al., 2009). Many components of dust, particularly iron and titanium oxides,

ACPD
12, 2303–2353, 2012

are photosensitive and show increased uptake and oxidation due to the formation of election-hole pairs (Nicolas et al., 2009; Ndour et al., 2009; Rubasinghege et al., 2010). The photoreactivity of Ti is supported by the lower fractionation factor for Factor 4 when exposed to O_3 or light as discussed in Sect. 5.3.4. There is no significant change in isotopic fractionation within any factor for the MDRHO3hv experiments, thus the increased sulfate production is not related to a change in mechanism. The combination of humidity, ozone and irradiation increases the rate of SO_2 oxidation, causing it to approach saturation. The experimental parameters can then have a significant impact on counteracting saturation of SO_2 uptake on dust, thus increasing the amount of SO_2 taken up and oxidised on the dust during the experiments. The rate is of uptake and oxidation is then approximately an order of magnitude higher than with any parameter alone.

6 Comparison to field studies

A number of studies have looked at isotopic ratios of sulfate in order to understand sulfur sources and oxidation pathways. As sulfur isotope fractionation factors have not been available for data interpretation, $\Delta^{17}O$ values are generally used to examine oxidation pathways. Oxidation by OH radicals and O_2 (which acts as the oxidant during transition metal catalysis) result in sulfate with $\Delta^{17}O = 0$ ‰, while oxidation by O_3 and H_2O_2 produces sulfate with $\Delta^{17}O = 8.8$ and 0.8 ‰, respectively (Savarino et al., 2000; Lee and Thiemens, 2001). Alexander et al. (2003) used $\Delta^{17}O$ measurements of sulfate in East Antarctic ice cores to show that oxidation by O_3 and H_2O_2 was less important in glacial periods than in the surrounding interglacials. $\delta^{34}S$ of sulfate is also lower during glacial periods, thus Harris et al. (2012) proposed an increase in transition-metal catalysed SO_2 oxidation due to increased dust loads in glacial periods, based on laboratory measurements of oxidation of SO_2 by Fe^{2+}/Fe^{3+} solutions. The results of this study show that sulfur isotope fractionation during oxidation by real mineral dust leachate

ACPD
12, 2303–2353, 2012

is equal to fractionation during oxidation by iron catalysis, although oxidation is much faster, thus supporting the hypothesis that oxidation by transition metal catalysis is ~27 % more important in glacial periods than in interglacial periods due to increased dust loads. Similarly, McCabe et al. (2006) measured $\Delta^{17}O$ of sulfate aerosol in Alert, Canada, and proposed that the importance of transition metal-catalysed oxidation was underestimated in winter, when concentrations of Fe and Mn are approximately doubled due to transport of polluted air masses. Norman et al. (1999) found that $\delta^{34}S$ of non-sea salt sulfate aerosol at Alert was lower in winter than in summer, which is consistent with the results of McCabe et al. (2006) when the fractionation factor for transition metal catalysis measured in this study is considered. Although the suite of transition metals from a polluted source will be different to those from a dust source, this study has shown that the identity of the transition metals involved in catalysis does not affect the isotopic fractionation.

In the majority of field studies, measured $\delta^{34}S$ of SO_2 is lower than $\delta^{34}S$ of sulfate (eg. Saltzman et al., 1983; Mukai et al., 2001; Novak et al., 2001). Thus, considering the fractionation factors from this study and from Harris et al. (2012), isotopic measurements are in agreement with modelling studies which show that transition metal catalysed oxidation of SO_2 contributes a minor part of global sulfate production. For example, Sofen et al. (2011) suggest the pathway contributes 18 % of sulfate production globally. Using the present-day partitioning between oxidation pathways from Sofen et al. (2011) and the sulfur isotope fractionation factors from this study and from Harris et al. (2012), we would predict a global average difference of +4.7 ‰ between $\delta^{34}S$ of SO_2 and $\delta^{34}S$ of sulfate. Considering a number of studies that simultaneously measured $\delta^{34}S$ of SO_2 and sulfate (Saltzman et al., 1983; Mayer et al., 1995; Krouse et al., 1991; Tanaka et al., 1994; Torfs et al., 1997; Mukai et al., 2001; Novak et al., 2001), the best estimate of the globally-averaged difference between $\delta^{34}S$ of SO_2 and $\delta^{34}S$ of sulfate is $+2.8 \pm 3.1$ ‰; this would require 36 % of oxidation to come from transition metal ion catalysis if the relative proportions of the other pathways remained the same. However, the area covered by these studies is mainly in Europe and North America,

ACPD
12, 2303–2353, 2012

and there are no measurements from the polar regions and the Southern Hemisphere, so the result may not be representative of the true global picture. There are currently no regional studies focussing on the isotopic composition of sulfate formed on dust, although there are a number of field studies that have confirmed the important role dust can play in regional sulfur cycles (Falkovich et al., 2001; Umann et al., 2005; Sullivan et al., 2007). The importance of uptake at lower relative humidities is not well known, and although it is slow compared to aqueous oxidation, its climatic role may be underestimated as dust does not generally encounter high humidity until some days after emission (Dentener et al., 1996). The fractionation factors presented in this study provide a new tool through which sulfur isotope measurements can be used to examine global and regional sulfur cycles, particularly the role of oxidation on clay minerals and in the aqueous phase.

7 Conclusions

The aim of this study was to measure fractionation of $^{34}S/^{32}S$ during oxidation of SO_2 by mineral dust leachate and on mineral dust surfaces, in order to better understand the role of SO_2 oxidation by mineral dust in the sulfur cycle. The fractionation factor α_{34} for oxidation in the leachate was $\alpha_{\text{leachate}} = 0.9917 \pm 0.0046$. Sulfate production was due to oxidation of SO_2 via the radical chain reaction pathway initiated by transition metal ions leached from the dust, and the oxidation rate was found to be more than 100 × faster than oxidation by iron alone.

Heterogeneous oxidation on dry and humidified dust surfaces lead to isotopic fractionation that was controlled primarily by the dust composition and not by the reaction parameters: $[O_3]$, irradiation, and humidity. However, almost an order of magnitude more sulfate was produced when the dust was simultaneously exposed to SO_2, O_3, humidity and light. Fractionation from different reactions occurring within the same $2\,\mu m^2$ area was additive, thus a multivariate analysis model could predict $\delta^{34}S$ of the sulfate produced on the grains within expected experimental error.

ACPD
12, 2303–2353, 2012

Not all particles reacted with SO_2, and the model identified the four major components of dust responsible for uptake and oxidation of SO_2. The most reactive components of dust were ilmenite, rutile and iron oxide, which produced sulfate with a fractionation factor of $\alpha_{34} = 1.012 \pm 0.010$. The overall fractionation factor on SDCV is $\alpha_{het} = 1.0096 \pm 0.0036$. Since the isotopic fractionation is controlled by the mineralogy of the dust, it will vary for dust from different dust source regions and between natural mineral dust and industrial dust sources.

The distinct fractionation factors for SO_2 oxidation by dust leachate – for example, in cloud droplets seeded on dust particles – and for uptake and oxidation on dust at subsaturated relative humidity will be particularly useful to investigate the relative importance of these two pathways as dust is transported. Although the aqueous reaction is much faster, the surface reaction may be fast enough to be important when the dust encounters O_3 and 30–40 % relative humidity in the daytime, whereas high enough humidities for aqueous oxidation are unlikely to be reached for several days following emission (Dentener et al., 1996). However, the isotopic fractionation during uptake and oxidation on Sahara dust surface, in particular on Ti and Fe oxides and silicates, does not significantly differ from the isotopic fractionation during gas phase oxidation of SO_2 by OH and oxidation by O_3 and H_2O_2 in the aqueous phase (Harris et al., 2012). Therefore, further from dust sources when high enough humidity for all of the possible oxidation pathways has been encountered, ambient observations for Sahara dust may only be capable of quantifying the contribution of leached transition metal ions and surface reactions on clay minerals to sulfate formation. The fractionation factor for SO_2 oxidation by transition metal catalysis is distinct from oxidation on the dust surface, other than feldspar minerals, and by H_2O_2 and O_3 in the aqueous phase and OH in the gas phase, and will provide a means to assess the global and regional importance of transition metal-catalysed SO_2 oxidation, by both dust TMIs and anthropogenic TMIs, which cannot be easily predicted from measurable parameters such as soluble iron concentration. Oxidation on feldspar minerals was found to be slow and would only present a minor interference for these calculations.

ACPD
12, 2303–2353, 2012

Acknowledgements. We thank Elmar Gröner for his support with the NanoSIMS analyses, Joachim Huth for his help with the SEM/EDX analyses, Robert Oswald for assistance in measuring O_3 concentrations and Christa Sudek for help with the ICP-OES analysis. This research was funded by the Max Planck Society and the Max Planck Graduate Centre.

The service charges for this open access publication have been covered by the Max Planck Society.

References

Adams, J. W., Rodriguez, D., and Cox, R. A.: The uptake of SO_2 on Saharan dust: a flow tube study, Atmos. Chem. Phys., 5, 2679–2689, doi:10.5194/acp-5-2679-2005, 2005. 2307, 2328

Al-Hosney, H. A. and Grassian, V. H.: Water, sulfur dioxide and nitric acid adsorption on calcium carbonate: a transmission and ATR-FTIR study, Phys. Chem. Chem. Phys., 7, 1266–1276, 2005. 2307, 2308, 2327, 2328

Alexander, B., Thiemens, M. H., Farquhar, J., Kaufman, A. J., Savarino, J., and Delmas, R. J.: East Antarctic ice core sulfur isotope measurements over a complete glacial-interglacial cycle, J. Geophys. Res.-Atmos., 108, 4786, doi:10.1029/2003JD003513, 2003. 2329

Baker, A. R., Jickells, T. D., Witt, M., and Linge, K. L.: Trends in the solubility of iron, aluminium, manganese and phosphorus in aerosol collected over the Atlantic Ocean RID D-1233-2011 RID B-2210-2010 RID B-8095-2008, Mar. Chem., 98, 43–58, doi:10.1016/j.marchem.2005.06.004, 2006. 2317

Bogumil, K., Orphal, J., Homann, T., Voigt, S., Spietz, P., Fleischmann, O. C., Vogel, A., Hartmann, M., Kromminga, H., Bovensmann, H., Frerick, J., and Burrows, J. P.: Measurements of molecular absorption spectra with the SCIAMACHY pre-flight model: instrument characterization and reference data for atmospheric remote-sensing in the 230–2380 nm region, J. Photochem. Photobio. A, 157, 167–184, 2003. 2347

Caquineau, S., Gaudichet, A., Gomes, L., and Legrand, M.: Mineralogy of Saharan dust transported over northwestern tropical Atlantic Ocean in relation to source regions, J. Geophys. Res.-Atmos., 107, 4251, doi:10.1029/2000JD000247, 2002. 2320

Cohen, S., Chang, S. G., Markowitz, S. S., and Novakov, T.: Role of fly ash in catalytic oxida-

ACPD

12, 2303–2353, 2012

tion of sulfur(IV) slurries, Environ. Sci. Technol., 15, 1498–1502, doi:10.1021/es00094a013, 1981. 2308, 2309, 2318

Coude-Gaussen, G., Rognon, P., and Le Coustumer, M.: Incorporation progressive de poussières sahariennes aux limons des les orientales du Cap Vert, C.R. Acad. Sci. II A, 319, 1343–1349, 1994. 2307, 2309, 2310, 2325, 2326, 2342

Crowley, J. N., Ammann, M., Cox, R. A., Hynes, R. G., Jenkin, M. E., Mellouki, A., Rossi, M. J., Troe, J., and Wallington, T. J.: Evaluated kinetic and photochemical data for atmospheric chemistry: Volume V – heterogeneous reactions on solid substrates, Atmos. Chem. Phys., 10, 9059–9223, doi:10.5194/acp-10-9059-2010, 2010. 2307, 2323, 2324, 2325, 2327

Cziczo, D. J., Froyd, K. D., Gallavardin, S. J., Moehler, O., Benz, S., Saathoff, H., and Murphy, D. M.: Deactivation of ice nuclei due to atmospherically relevant surface coatings, Environ. Res. Lett., 4, 044013, doi:10.1088/1748-9326/4/4/044013, 2009. 2305

Dentener, F. J., Carmichael, G. R., Zhang, Y., Lelieveld, J., and Crutzen, P. J.: Role of mineral aerosol as a reactive surface in the global troposphere, J. Geophys. Res.-Atmos., 101, 22869–22889, 1996. 2305, 2331, 2332

Derda, M., Chmielewski, A. G., and Licki, J.: Sulphur isotope compositions of components of coal and S-isotope fractionation during its combustion and flue gas desulphurization, Isot. Environ. Health S., 43, 57–63, 2007. 2312

Ding, T., Valkiers, S., Kipphardt, H., De Bievre, P., Taylor, P. D. P., Gonfiantini, R., and Krouse, R.: Calibrated sulfur isotope abundance ratios of three IAEA sulfur isotope reference materials and V-CDT with a reassessment of the atomic weight of sulfur, Geochim. Cosmochim. Ac., 65, 2433–2437, 2001. 2306

Drake, N. A., Eckardt, F. D., and White, K. H.: Sources of sulphur in gypsiferous sediments and crusts and pathways of gypsum redistribution in Southern Tunisia, Earth Surf. Proc. Land., 29, 1459–1471, doi:10.1002/esp.1133, 2004. 2314

Falkovich, A. H., Ganor, E., Levin, Z., Formenti, P., and Rudich, Y.: Chemical and mineralogical analysis of individual mineral dust particles, J. Geophys. Res.-Atmos., 106, 18029–18036, 2001. 2320, 2321, 2331

Faust, B. C., Hoffmann, M. R., and Bahnemann, D. W.: Photocatalytic oxidation of sulfur-dioxide in aqueous suspensions of alpha-Fe_2O_3, J. Phys. Chem., 93, 6371–6381, 1989. 2308

Fu, H. B., Wang, X., Wu, H. B., Yin, Y., and Chen, J. M.: Heterogeneous uptake and oxidation of SO_2 on iron oxides, J. Phys. Chem. C, 111, 6077–6085, doi:10.1021/jp070087b, 2007. 2324

ACPD

12, 2303–2353, 2012

Gasso, S., Grassian, V. H., and Miller, R. L.: Interactions between mineral dust, climate, and ocean ecosystems, Elements, 6, 247–252, doi:10.2113/gselements.6.4.247, 2010. 2305
Glaccum, R. A. and Prospero, J. M.: Saharan aerosols over the tropical North Atlantic – mineralogy, Mar. Geol., 37, 295–321, doi:10.1016/0025-3227(80)90107-3, 1980. 2325, 2326
Goldstein, J., Newbury, D. E., Echlin, P., Joy, D., Fiori, C., and Lifshin, E.: Scanning Electron Microscopy and X-ray Microanalysis, Plenum Press, New York, 1981. 2313, 2319
Goodman, A. L., Li, P., Usher, C. R., and Grassian, V. H.: Heterogeneous uptake of sulfur dioxide on aluminum and magnesium oxide particles, J. Phys. Chem. A, 105, 6109–6120, 2001. 2307, 2325
Goodsel, A. J., Low, M. J. D., and Takezawa, N.: Reactions of gaseous pollutants with solids. II. Infrared study of sorption of sulfur dioxide on magnesium oxide, Environ. Sci. Technol., 6, 268–273, doi:10.1021/es60062a001, 1972. 2327
Groener, E. and Hoppe, P.: Automated ion imaging with the NanoSIMS ion microprobe, Appl. Surf. Sci., 252, 7148–7151, doi:10.1016/j.apsusc.2006.02.280, 2006. 2313
Gustafsson, R. J., Orlov, A., Badger, C. L., Griffiths, P. T., Cox, R. A., and Lambert, R. M.: A comprehensive evaluation of water uptake on atmospherically relevant mineral surfaces: DRIFT spectroscopy, thermogravimetric analysis and aerosol growth measurements, Atmos. Chem. Phys., 5, 3415–3421, doi:10.5194/acp-5-3415-2005, 2005. 2311
Hanisch, F. and Crowley, J. N.: Heterogeneous reactivity of gaseous nitric acid on Al_2O_3, $CaCO_3$, and atmospheric dust samples: a Knudsen cell study, J. Phys. Chem. A, 105, 3096–3106, 2001. 2307, 2309, 2312
Hanisch, F. and Crowley, J. N.: Ozone decomposition on Saharan dust: an experimental investigation, Atmos. Chem. Phys., 3, 119–130, doi:10.5194/acp-3-119-2003, 2003. 2307, 2309, 2313, 2328, 2342
Harris, E., Sinha, B., Hoppe, P., Crowley, J. N., Ono, S., and Foley, S.: Sulfur isotope fractionation during oxidation of sulfur dioxide: gas-phase oxidation by OH radicals and aqueous oxidation by H_2O_2, O_3 and iron catalysis, Atmos. Chem. Phys., 12, 407–423, doi:10.5194/acp-12-407-2012, 2012. 2306, 2310, 2312, 2313, 2315, 2317, 2318, 2329, 2330, 2332
Heinold, B., Tegen, I., Esselborn, M., Kandler, K., Knippertz, P., Mueller, D., Schadlitz, A., Tesche, M., Weinzerl, B., Ansmann, A., Althausen, D., Laurent, B., Massling, A., Mueller, T., Petzold, A., Schepanski, K., and Wiedensohler, A.: Regional Saharan dust modelling during the SAMUM 2006 campaign, Tellus B, 61, 307–324, doi:10.1111/j.1600-0889.2008.00387.x, 2009. 2309

ACPD
12, 2303–2353, 2012

Herrmann, H., Ervens, B., Jacobi, H. W., Wolke, R., Nowacki, P., and Zellner, R.: CAPRAM2.3: a chemical aqueous phase radical mechanism for tropospheric chemistry, J. Atmos. Chem., 36, 231–284, 2000. 2319, 2325

Hong, A. P., Bahnemann, D. W., and Hoffmann, M. R.: Cobalt(ii) tetrasulfophthalocyanine on titanium-dioxide .2. Kinetics and mechanisms of the photocatalytic oxidation of aqueous sulfur-dioxide, J. Phys. Chem., 91, 6245–6251, doi:10.1021/j100308a035, 1987. 2308

Hoppe, P.: NanoSIMS: a new tool in cosmochemistry, Appl. Surf. Sci., 252, 7102–7106, 2006. 2313

Janssen, A., Geisler, T., Putnis, C., and Putnis, A.: The mechanism of oxidation and "leaching" of ilmenite during natural and experimental alteration, Geochim. Cosmochim. Ac., 71, A440–A440, 2007. 2324

Jayne, J. T., Davidovits, P., Worsnop, D. R., Zahniser, M. S., and Kolb, C. E.: Uptake of SO_2 (g) by aqueous surfaces as a function of pH – the effect of chemical-reaction at the interface, J. Phys. Chem., 94, 6041–6048, doi:10.1021/j100378a076, 1990. 2323

Jickells, T. D., An, Z. S., Andersen, K. K., Baker, A. R., Bergametti, G., Brooks, N., Cao, J. J., Boyd, P. W., Duce, R. A., Hunter, K. A., Kawahata, H., Kubilay, N., laRoche, J., Liss, P. S., Mahowald, N., Prospero, J. M., Ridgwell, A. J., Tegen, I., and Torres, R.: Global iron connections between desert dust, ocean biogeochemistry, and climate, Science, 308, 67–71, 2005. 2305

Judeikis, H. S., Stewart, T. B., and Wren, A. G.: Laboratory studies of the heterogeneous reactions of SO_2, Atmos. Environ., 12, 1633–1641, 1978. 2307, 2325, 2328

Kaaden, N., Massling, A., Schladitz, A., Mueller, T., Kandler, K., Schuetz, L., Weinzierl, B., Petzold, A., Tesche, M., Leinert, S., Deutscher, C., Ebert, M., Weinbruch, S., and Wiedensohler, A.: State of mixing, shape factor, number size distribution, and hygroscopic growth of the Saharan anthropogenic and mineral dust aerosol at Tinfou, Morocco, Tellus B, 61, 51–63, doi:10.1111/j.1600-0889.2008.00388.x, 2009. 2305, 2309

Karge, H. G. and Dalla Lana, I. G.: Infrared studies of SO_2 adsorption on a Claus catalyst by selective poisoning of sites, J. Phys. Chem., 88, 1538–1543, 1984. 2325

Kim, B. G. and Park, S. U.: Transport and evolution of a winter-time yellow sand observed in Korea, Atmos. Environ., 35, 3191–3201, doi:10.1016/S1352-2310(00)00469-6, 2001. 2305

Krouse, H. R. and Grinenko, V. A. (Eds.): Stable Isotopes: Natural and Anthropogenic Sulphur in the Environment, Vol. 43, Wiley, Chichester, 1991. 2316, 2317, 2318

Krouse, H., Grinenko, L., Grinenko, V., Newman, L., Forrest, J., Nakai, N., Tsuji, Y., Yatsum-

ACPD
12, 2303–2353, 2012

imi, T., Takeuchi, V., Robinson, B., Stewart, M., Gunatilaka, A., Plumb, L., Smith, J., Buzek, F., Cerny, J., Sramek, J., Menon, A., Iyer, G., Venkatasubramanian, V., Egboka, B., Irogbenachi, M., and Eligwe, C.: Case studies and potential applications, in: Stable Isotopes: Natural and Anthropogenic Sulphur in the Environment, Chap. 8., edited by: Krouse, H. R. and Grinenko, V. A., John Wiley and Sons, Chichester, 307–416, 1991. 2330

Kumar, A. and Sarin, M. M.: Aerosol iron solubility in a semi-arid region: temporal trend and impact of anthropogenic sources, Tellus Series B-chemical and Physical Meteorology, 62, 125–132, doi:10.1111/j.1600-0889.2009.00448.x, 2010. 2317

Kumar, A., Sarin, M. M., and Srinivas, B.: Aerosol iron solubility over Bay of Bengal: role of anthropogenic sources and chemical processing, Mar. Chem., 121, 167–175, doi:10.1016/j.marchem.2010.04.005, 2010. 2305, 2308

Lee, C. C. W. and Thiemens, M. H.: The δO-17 and δO-18 measurements of atmospheric sulfate from a coastal and high alpine region: a mass-independent isotopic anomaly, J. Geophys. Res.-Atmos., 106, 17359–17373, 2001. 2329

Levin, Z., Ganor, E., and Gladstein, V.: The effects of desert particles coated with sulfate on rain formation in the Eastern Mediterranean, Journal of Applied Meteorology, 35, 1511–1523, 1996. 2305

Li, L., Chen, Z. M., Zhang, Y. H., Zhu, T., Li, J. L., and Ding, J.: Kinetics and mechanism of heterogeneous oxidation of sulfur dioxide by ozone on surface of calcium carbonate, Atmos. Chem. Phys., 6, 2453–2464, doi:10.5194/acp-6-2453-2006, 2006. 2308, 2327, 2328

Li, L., Chen, Z. M., Zhang, Y. H., Zhu, T., Li, S., Li, H. J., Zhu, L. H., and Xu, B. Y.: Heterogeneous oxidation of sulfur dioxide by ozone on the surface of sodium chloride and its mixtures with other components, J. Geophys. Res.-Atmos., 112, D18301, doi:10.1029/2006JD008207, 2007. 2326

Liao, H. and Seinfeld, J. H.: Global impacts of gas-phase chemistry-aerosol interactions on direct radiative forcing by anthropogenic aerosols and ozone, J. Geophys. Res.-Atmos., 110, D18208, doi:10.1029/2005JD005907, 2005. 2306

Lin, Y., Sim, M. S., and Ono, S.: Multiple-sulfur isotope effects during photolysis of carbonyl sulfide, Atmos. Chem. Phys., 11, 10283–10292, doi:10.5194/acp-11-10283-2011, 2011. 2312

Low, M. J. D., Goodsel, A. J., and Takezawa, N.: Reactions of gaseous pollutants with solids. I. Infrared study of the sorption of sulfur dioxide on calcium oxide, Environ. Sci. Technol., 5, 1191–1195, doi:10.1021/es60059a003, 1971. 2327

Mamane, Y. and Gottlieb, J.: Heterogeneous reactions of minerals with sulfur and nitrogen

ACPD
12, 2303–2353, 2012

oxides, Journal of Aerosol Science, 20, 303–311, 1989. 2328
Mariotti, A., Germon, J. C., Hubert, P., Kaiser, P., Letolle, R., Tardieux, A., and Tardieux, P.: Experimental-determination of nitrogen kinetic isotope fractionation – some principles – illustration for the denitrification and nitrification processes, Plant and Soil, 62, 413–430, 1981. 2316, 2317, 2318
Mayer, B., Feger, K. H., Giesemann, A., and Jäger, H. J.: Interpretation of sulfur cycling in two catchments in the Black Forest (Germany) using stable sulfur and oxygen isotope data, Biogeochemistry, 30, 31–58, 1995. 2330
McCabe, J. R., Savarino, J., Alexander, B., Gong, S. L., and Thiemens, M. H.: Isotopic constraints on non-photochemical sulfate production in the Arctic winter, Geophysical Research Letters, 33, L05810, doi:10.1029/2005GL025164, 2006. 2330
Morales, C.: The airborne transport of Saharan dust: a review, Climatic Change, 9, 219–241, doi:10.1007/BF00140538, 1986. 2305, 2309
Mukai, H., Tanaka, A., Fujii, T., Zeng, Y. Q., Hong, Y. T., Tang, J., Guo, S., Xue, H. S., Sun, Z. L., Zhou, J. T., Xue, D. M., Zhao, J., Zhai, G. H., Gu, J. L., and Zhai, P. Y.: Regional characteristics of sulfur and lead isotope ratios in the atmosphere at several Chinese urban sites, Environ. Sci. Technol., 35, 1064–1071, 2001. 2330
Ndour, M., Nicolas, M., D'Anna, B., Ka, O., and George, C.: Photoreactivity of NO_2 on mineral dusts originating from different locations of the Sahara desert, Phys. Chem. Chem. Phys., 11, 1312–1319, 2009. 2329
Nicolas, M., Ndour, M., Ka, O., D'Anna, B., and George, C.: Photochemistry of atmospheric dust: ozone decomposition on illuminated titanium dioxide, Environ. Sci. Technol., 43, 7437–7442, 2009. 2308, 2328, 2329
Norman, A. L., Barrie, L. A., Toom-Sauntry, D., Sirois, A., Krouse, H. R., Li, S. M., and Sharma, S.: Sources of aerosol sulphate at alert: apportionment using stable isotopes, J. Geophys. Res.-Atmos., 104, 11619–11631, 1999. 2330
Norris, G., Vedantham, R., Wade, K., Brown, S., Prouty, J., and Foley, C.: EPA Positive Matrix Factorization (PMF) 3.0 Fundamentals and User Guide, US Environmental Protection Agency, Office of Research and Development, Washington, DC, 2008. 2315, 2316
Novak, M., Jackova, I., and Prechova, E.: Temporal trends in the isotope signature of air-borne sulfur in Central Europe, Environ. Sci. Technol., 35, 255–260, 2001. 2330
Pacchioni, G., Clotet, A., and Ricart, J. M.: A theoretical study of the absorption and reaction of SO_2 at surface and step sites of the MgO(100) surface, Surface Science, 315, 337–350,

ACPD
12, 2303–2353, 2012

1994. 2307
Park, S. H., Song, C. B., Kim, M. C., Kwon, S. B., and Lee, K. W.: Study on size distribution of total aerosol and water-soluble ions during an Asian dust storm event at Jeju Island, Korea, Environmental Monitoring and Assessment, 93, 157–183, doi:10.1023/B:EMAS.0000016805.04194.56, 2004. 2305
Pruppacher, H. and Klett, J.: Microphysics of Clouds and Precipitation, 2nd edn., Kluwer Academic Publishers, Dordrecht, The Netherlands, 1997. 2305
Putnis, A.: Mineral replacement reactions: from macroscopic observations to microscopic mechanisms, Mineralogical Magazine, 66, 689–708, doi:10.1180/0026461026650056, 2002. 2324
Rani, A., Prasad, D. S. N., Madnawat, P. V. S., and Gupta, K. S.: The role of free-fall atmospheric dust in catalyzing autoxidation of aqueous sulfur-dioxide, Atmos. Environ. A-Gen., 26, 667–673, 1992. 2308, 2309, 2317, 2318
Roithner: Preliminary Information: Hexagonal High-Power UV LED H2A1 UV Series, Roithner Lasertechnik GmbH, Vienna, Austria, available at: http://www.roithner-laser.com/datasheets/led_single/hexagonal/h2a1-uv.pdf, last access: August 2011. 2347
Rubasinghege, G., Elzey, S., Baltrusaitis, J., Jayaweera, P. M., and Grassian, V. H.: Reactions on atmospheric dust particles: surface photochemistry and size-dependent nanoscale redox chemistry, J. Phys. Chem. Lett., 1, 1729–1737, 2010. 2305, 2329
Rufus, J., Stark, G., Smith, P. L., Pickering, J. C., and Thorne, A. P.: High-resolution photoabsorption cross section measurements of SO_2, 2: 220 to 325 nm at 295 K, J. Geophys. Res., 108, 5011, doi:10.1029/2002JE001931, 2003. 2347
Saltzman, E. S., Brass, G., and Price, D.: The mechanism of sulfate aerosol formation: chemical and sulfur isotopic evidence, Geophys. Res. Lett., 10, 513–516, 1983. 2330
Savarino, J., Lee, C. C. W., and Thiemens, M. H.: Laboratory oxygen isotopic study of sulfur (IV) oxidation: origin of the mass-independent oxygen isotopic anomaly in atmospheric sulfates and sulfate mineral deposits on Earth, J. Geophys. Res.-Atmos., 105, 29079–29088, 2000. 2329
Sofen, E. D., Alexander, B., and Kunasek, S. A.: The impact of anthropogenic emissions on atmospheric sulfate production pathways, oxidants, and ice core $\Delta^{17}O(SO_4^{2-})$, Atmos. Chem. Phys., 11, 3565–3578, doi:10.5194/acp-11-3565-2011, 2011. 2330
Sullivan, R. C., Guazzotti, S. A., Sodeman, D. A., and Prather, K. A.: Direct observations of the atmospheric processing of Asian mineral dust, Atmos. Chem. Phys., 7, 1213–1236,

ACPD
12, 2303–2353, 2012

doi:10.5194/acp-7-1213-2007, 2007. 2331
Tanaka, T. Y. and Chiba, M.: A numerical study of the contributions of dust source regions to the global dust budget, Global Planet. Change, 52, 88–104, doi:10.1016/j.gloplacha.2006.02.002, 2006. 2305, 2306
Tanaka, N., Rye, D. M., Xiao, Y., and Lasaga, A. C.: Use of stable sulfur isotope systematics for evaluating oxidation reaction pathways and in-cloud scavenging of sulfur-dioxide in the atmosphere, Geophys. Res. Lett., 21, 1519–1522, 1994. 2330
Tilly, J., Lewicki, M., Tomaszewski, Z., and Toczkowski, J.: Use of ilmenite decomposition products in a gas desulfurization process, J. Chem. Technol. Biot., 52, 301–310, 1991. 2308, 2317, 2318
Torfs, K. M., VanGrieken, R., and Buzek, F.: Use of stable isotope measurements to evaluate the origin of sulfur in gypsum layers on limestone buildings, Environ. Sci. Technol., 31, 2650–2655, 1997. 2330
Ullerstam, M., Vogt, R., Langer, S., and Ljungstrom, E.: The kinetics and mechanism of SO_2 oxidation by O-3 on mineral dust, Phys. Chem. Chem. Phys., 4, 4694–4699, 2002. 2307, 2308, 2328
Ullerstam, M., Johnson, M. S., Vogt, R., and Ljungström, E.: DRIFTS and Knudsen cell study of the heterogeneous reactivity of SO_2 and NO_2 on mineral dust, Atmos. Chem. Phys., 3, 2043–2051, doi:10.5194/acp-3-2043-2003, 2003. 2307, 2308
Umann, B., Arnold, F., Schaal, C., Hanke, M., Uecker, J., Aufmhoff, H., Balkanski, Y., and Dingenen, R. V.: Interaction of mineral dust with gas phase nitric acid and sulfur dioxide during the MINATROC II field campaign: first estimate of the uptake coefficient $\gamma(HNO_3)$ from atmospheric data, J. Geophys. Res.-Atmos., 110, D22306, doi:10.1029/2005JD005906, 2005. 2331
Usher, C. R., Al-Hosney, H., Carlos-Cuellar, S., and Grassian, V. H.: A laboratory study of the heterogeneous uptake and oxidation of sulfur dioxide on mineral dust particles, J. Geophys. Res.-Atmos., 107, 4713, doi:10.1029/2002JD002051, 2002. 2307, 2308, 2324, 2326, 2327
Wagner, F., Bortoli, D., Pereira, S., Costa, M., Silva, A., Weinzierl, B., Esselborn, M., Petzold, A., Rasp, K., Heinold, B., and Tegen, I.: Properties of dust aerosol particles transported to Portugal from the Sahara desert, Tellus B, 61, 297–306, doi:10.1111/j.1600-0889.2008.00393.x, 2009. 2309
Winterholler, B.: Sulfur Isotope Analysis of Aerosol Particles by NanoSIMS, Ph.D. thesis, Johannes Gutenberg-Universität, Mainz, 2007. 2312

ACPD
12, 2303–2353, 2012

Winterholler, B., Hoppe, P., Andreae, M. O., and Foley, S.: Measurement of sulfur isotope ratios in micrometer-sized samples by NanoSIMS, Appl. Surf. Sci., 252, 7128–7131, 2006. 2313, 2314

Winterholler, B., Hoppe, P., Foley, S., and Andreae, M. O.: Sulfur isotope ratio measurements of individual sulfate particles by NanoSIMS, Int. J. Mass Spectrom., 272, 63–77, 2008. 2313, 2314

Xiao, H., Carmichael, G. R., Durchenwald, J., Thornton, D., and Bandy, A.: Long-range transport of SO_x and dust in East Asia during the PEM B experiment, J. Geophys. Res.-Atmos., 102, 28589–28612, 1997. 2305

Zender, C., Newman, D., and Tegen, I.: Quantifying mineral dust mass budgets: terminology, constraints, and current estimates, EOS T. Am. Geophys. Un., 85, 509–512, doi:10.1029/2004EO480002, 2004. 2305

Zhang, X. Y., Zhuang, G. S., Chen, J. M., Wang, Y., Wang, X., An, Z. S., and Zhang, P.: Heterogeneous reactions of sulfur dioxide on typical mineral particles, J. Phys. Chem. B, 110, 12588–12596, 2006. 2324, 2325, 2326, 2327

Zhu, S., Butler, T., Sander, R., Ma, J., and Lawrence, M. G.: Impact of dust on tropospheric chemistry over polluted regions: a case study of the Beijing megacity, Atmos. Chem. Phys., 10, 3855–3873, doi:10.5194/acp-10-3855-2010, 2010. 2305

ACPD

12, 2303–2353, 2012

Table 1. Composition and mineralogy of SDCV adapted from Hanisch and Crowley (2003) and Coude-Gaussen et al. (1994), respectively.

Elemental composition	O	Si	Al	Mg	Ca	Fe	Ti	K	Na	Mn	P	S
Concentration (mg g^{-1} dust)	556.9	172.4	72.9	24.1	28.0	89.4	21.1	16.2	12.2	1.8	2.0	0.9

Mineralogy of clay fraction	Kaolinite	Smectite	Swelling chlorite	Chlorite	Illite
Abundance (%)	34.3	10.5	14.2	7.9	30.3

ACPD
12, 2303–2353, 2012

Table 2. Experiments to investigate isotopic fractionation during oxidation of SO_2 on the surface of mineral dust.

Abbreviation	O_3	Light	Humidity	Run	Length (h)
MDdark	no	no	no	1	7.9
				2	7.2
MDO3	yes	no	no	1	7.9
				2	9.2
MDhv	no	yes	no	1	8.2
				2	8.2
MDO3hv	yes	yes	no	1	7.8
				2	7.7
MDRHdark	no	no	yes	1	7.8
				2	8.3
MDRHO3	yes	no	yes	1	7.5
				2	7.9
MDRHhv	no	yes	yes	1	6.7
				2	7.3
MDRHO3hv	yes	yes	yes	1	6.3
				2	7.5

ACPD
12, 2303–2353, 2012

Table 3. The concentrations of various elements present in Sahara dust leachate measured with ICP-OES. "Concentration" refers to the solution used to oxidise SO_2 in this study, which was made with 0.5 g of dust per 100 ml of water, while "$\mu g\, g^{-1}$ dust" is the amount of the element that is soluble in 1 g of dust following 2 days in MilliQ water. "RSD" is the relative standard deviation of 3 measurements from the ICP-OES.

Element	Concentration $mol\, l^{-1}$	$\mu g\, g^{-1}$ dust	RSD %
Al	3.19×10^{-5}	170	3.7
Mg	1.61×10^{-5}	77.1	3.1
Ca	1.53×10^{-5}	121	2.8
Fe	7.74×10^{-6}	85.2	8.4
Ba	2.64×10^{-6}	71.5	1.9
Ti	2.22×10^{-6}	20.9	1.3
Mn	7.48×10^{-7}	8.09	4.1
Sr	1.43×10^{-7}	2.47	0.95
Cr	6.2×10^{-8}	0.64	160
Ni	3.4×10^{-9}	0.04	840

ACPD
12, 2303–2353, 2012

Table 4. Fractionation of $^{34}S/^{32}S$ during heterogeneous oxidation of SO_2 (g) on mineral dust surfaces. "Sulfate production" shows the percentage of the total sulfate production contributed by the factor while "Reactivity" shows the amount of sulfate produced per gram of the minerals represented by the factor per hour of reaction time at an SO_2 concentration of 4.2 ppm for MDRHO3hv experiments. γ is the reactive uptake coefficient considering the BET surface area of the dust for MDRHO3hv experiments.

Factor	Sulfate production %	Reactivity µg sulfate/g minerals/h	γ_{obs}	Mineralogy	α_{34}
1	85.0	12.6	3×10^{-5}	ilmenite + rutile	1.012 ± 0.010
2	3.2	0.40	9×10^{-7}	feldspar	0.948 ± 0.012
3	0.1	0.05	4×10^{-8}	silicates + basic components (eg. MgO)	1.007 ± 0.011
4	11.7	2.91	9×10^{-6}	clay (chlorite, illite, smectite)	1.085 ± 0.013

ACPD
12, 2303–2353, 2012

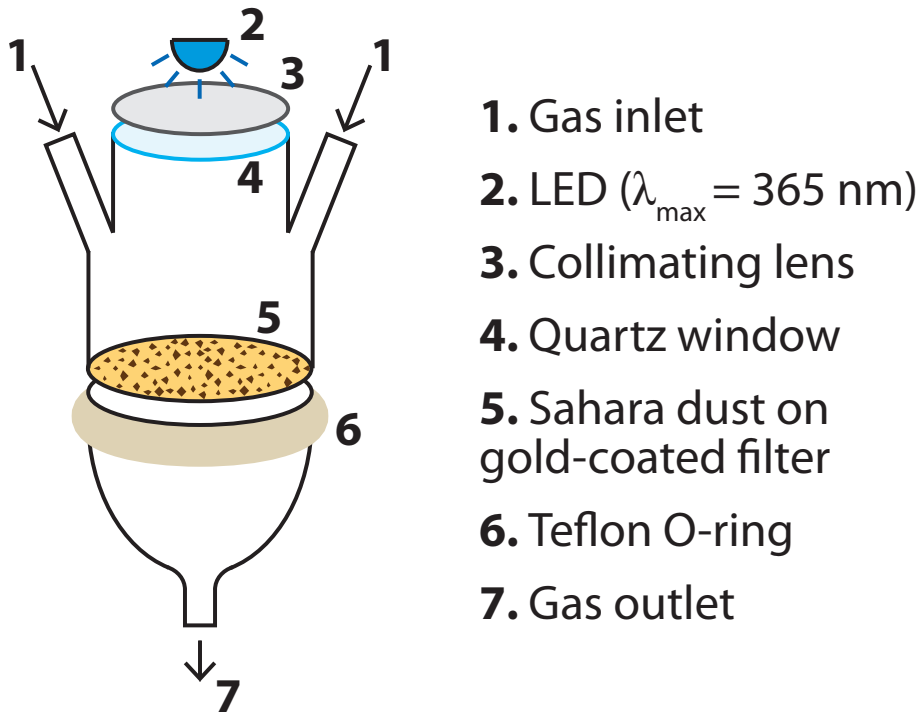

Fig. 1. Reactor used to investigate fractionation during oxidation of SO_2 on mineral dust.

ACPD
12, 2303–2353, 2012

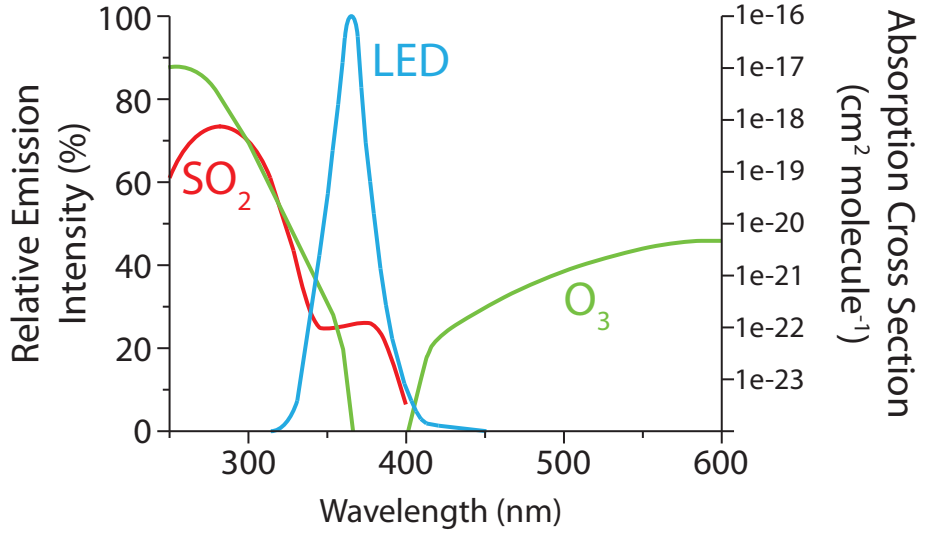

Fig. 2. Emission spectrum of LED used to irradiate mineral dust samples (blue line, left axis, Roithner (2011)) and absorption spectra of SO_2 (red line, right axis, Rufus et al., 2003) and O_3 (green line, right axis, Bogumil et al., 2003).

ACPD
12, 2303–2353, 2012

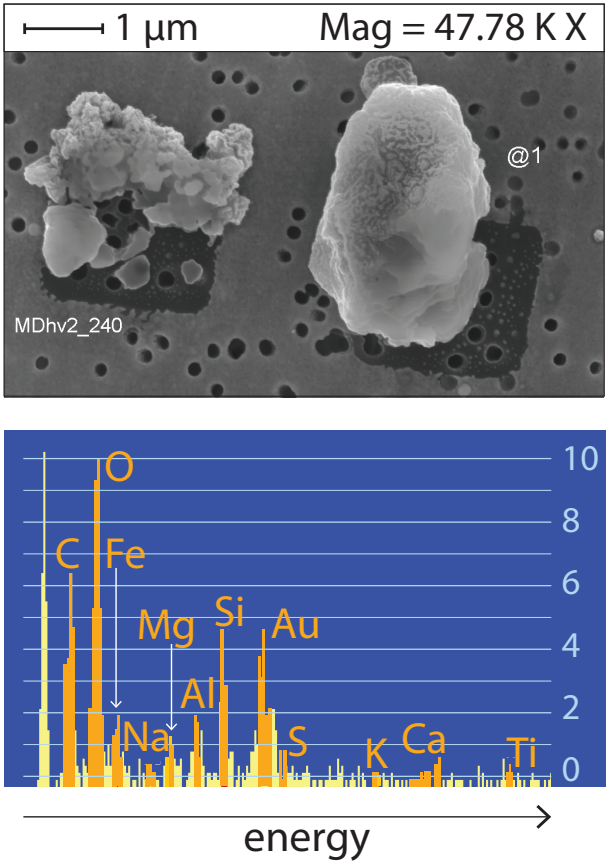

Fig. 3. SEM and EDX analysis of a mineral dust grain (right-hand grain) following a NanoSIMS measurement. The dark squares on the filter in the SEM image show where the NanoSIMS analysis has sputtered away the gold-coating. In the SEM EDX spectrum, element windows are highlighted in orange while the background is shown in yellow.

ACPD
12, 2303–2353, 2012

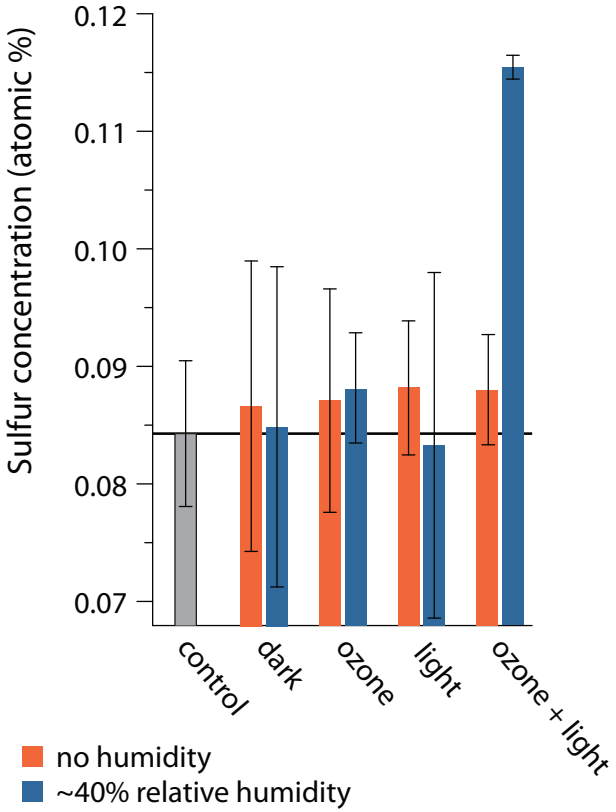

Fig. 4. Quantification of sulfate addition to mineral dust from surface SO_2 oxidation. "Control" shows the amount of sulfate present in untreated dust, and the labels on the *y*-axis refer to the different experimental conditions under which SO_2 was exposed to the dust. Error bars are the 1σ standard deviation from the Poisson distribution depending on the number of points with a significant signal.

ACPD
12, 2303–2353, 2012

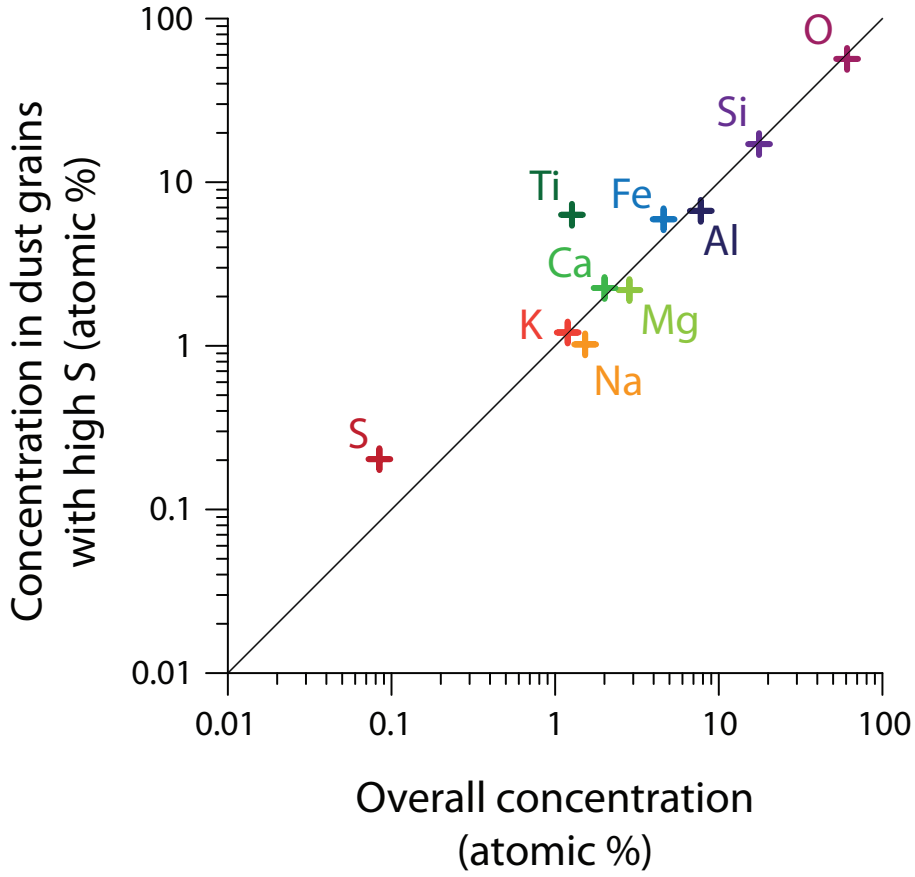

Fig. 5. Comparison of elemental composition of all dust and composition of dust with ^{32}S count rates high enough for reliable isotopic analysis.

ACPD
12, 2303–2353, 2012

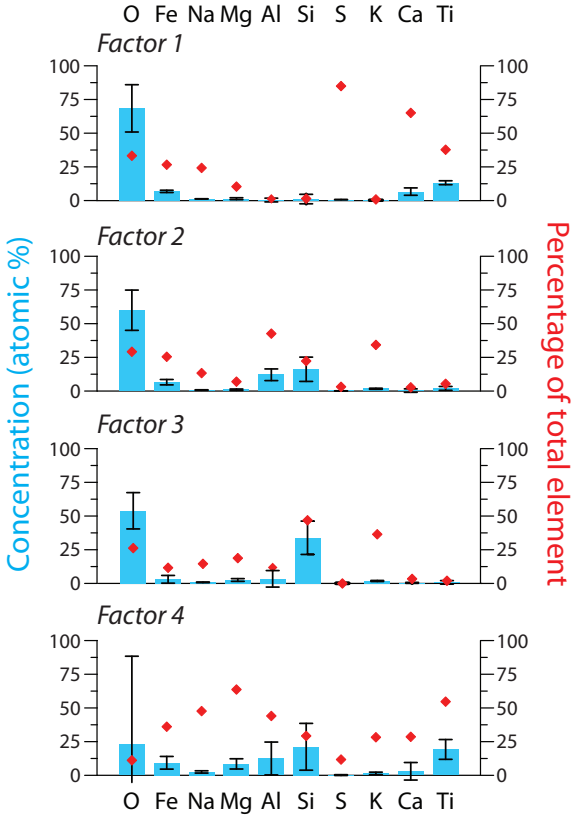

Fig. 6. Elemental profiles of the four "factors" contributing to isotopic composition of sulfate produced from SO_2 oxidation, identified by PMF analysis. Columns with 1σ error bars (standard deviation of the results of 20 model runs) correspond to the left-hand axis and show the concentration of the element in atomic percent, while diamonds correspond to the right-hand axis and show the percentage of the element's total concentration that is present in a particular factor.

ACPD
12, 2303–2353, 2012

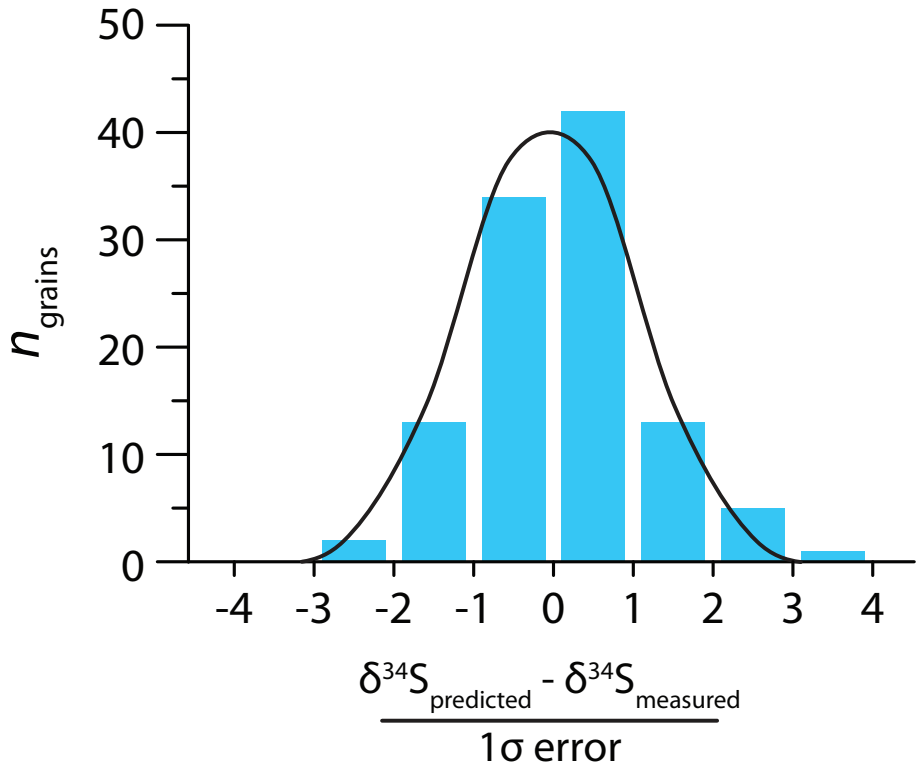

Fig. 7. Comparison of model accuracy (blue bars) with expected error from a normal distribution (black line).

ACPD
12, 2303–2353, 2012

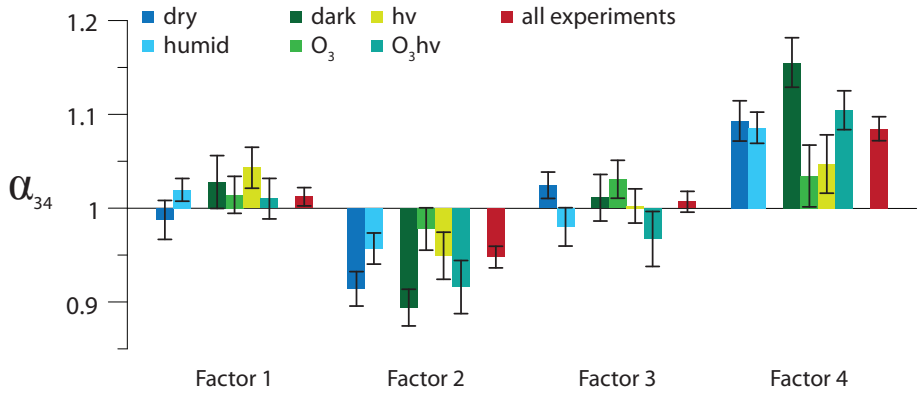

Fig. 8. Fractionation factors for $^{34}S/^{32}S$ for different mineral assemblages ("Factors") within Sahara dust: "dry" includes MDdark, MDO3, MDhv and MDO3hv, "humid" includes MDRHdark, MDRHO3, MDRHhv and MDRHO3hv; "dark" includes MDdark and MDRHdark, "hv" includes MDhv and MDRHhv, "O_3" includes MDO3 and MDRHO3, and "O_3hv" includes MDO3hv and MDRHO3hv. Error bars show the 1σ error.

ACPD
12, 2303–2353, 2012